CRANFIELD UNIVERSITY

Iñigo Gómez Goenaga

Bolted flange connections: friction and room temperature creep analysis

School of Water, Energy and Environment (SWEE)

MSc in Renewable Energy Engineering (REE)
Academic Year: 2017 - 2018

Supervisor: Dr Ali Mehmanparast

August 2018

CRANFIELD UNIVERSITY

School of Water, Energy and Environment (SWEE)

MSc in Renewable Energy Engineering (REE)

Academic Year 2017 - 2018

Iñigo Gómez Goenaga

Bolted flange connections: friction and room temperature creep analysis

Supervisor: Dr Ali Mehmanparast

August 2018

ABSTRACT

The scope of this project is the study of the foundation flange of an offshore wind turbine, and more precisely, the M72 bolts securing its position against internal and external loads. The project will focus on the M72 bolts themselves and different sources causing preload scatter and short-term relaxation. The first set of analysis will try to determine the influence of friction coefficients of the different contact surfaces in the flange. General reaction of the bolt, alongside local effects on the thread will be studied. On the other hand, an analysis of the influence of room temperature creep on short-term relaxation will follow. In spite of being usually neglected, the significant loads compared to yield appearing on the bolt may lead to creep strain rates that should not be neglected. In order to achieve positive results, a fully detailed FEA of a one-bolt segment of the flange will be developed. Material properties will be obtained based on information available in the literature, as well as the creep properties. Following this, a sensitivity analysis on both friction and creep properties will clarify the influence of these two factors in bolt's operation.

Keywords:

Abaqus

Bainite

Creep power law

Martensite

Ramberg-Osgood

Short-term relaxation

TABLE OF CONTENTS

LIST OF FIGURES

LIST OF TABLES

LIST OF EQUATIONS

LIST OF ABBREVIATIONS

O&M	Operation and maintenance
RO	Ramberg-Osgood
RT	Room Temperature
LT	Low Temperature
EXT	External contacts
TT	Thread to thread contact
FF	Flange to flange contact
$\dot{\varepsilon}_{cr}$	Creep strain rate
μ	Friction coefficient
σ_Y	Yield stress

1 INTRODUCTION

1.1 Offshore wind energy: economic status and prospects

The total power installed of offshore wind turbines by 2016 was close to 14.5 GW, being Europe the market leader in power capacity, with around 88% of the total. This is distributed in 10 different countries, among which the United Kingdom is the leading installer, with a total of 5.1 GW (over one third of global capacity) distributed in 27 wind farms [1].

In addition to that leadership, UK government plans to reach 25 GW installed (five times its actual capacity) by 2030 in pursue of a greener and more sustainable economy [2]. This increase in installed capacity is backed up by the efficiency of the electricity produced, having the UK offshore wind farms achieved the target of 100£/MWh in 2016, whereas this objective, which is known as Levelized Cost of Energy (LCOE) was set for 2020 [3]. Therefore, huge investments are expected in the close future.

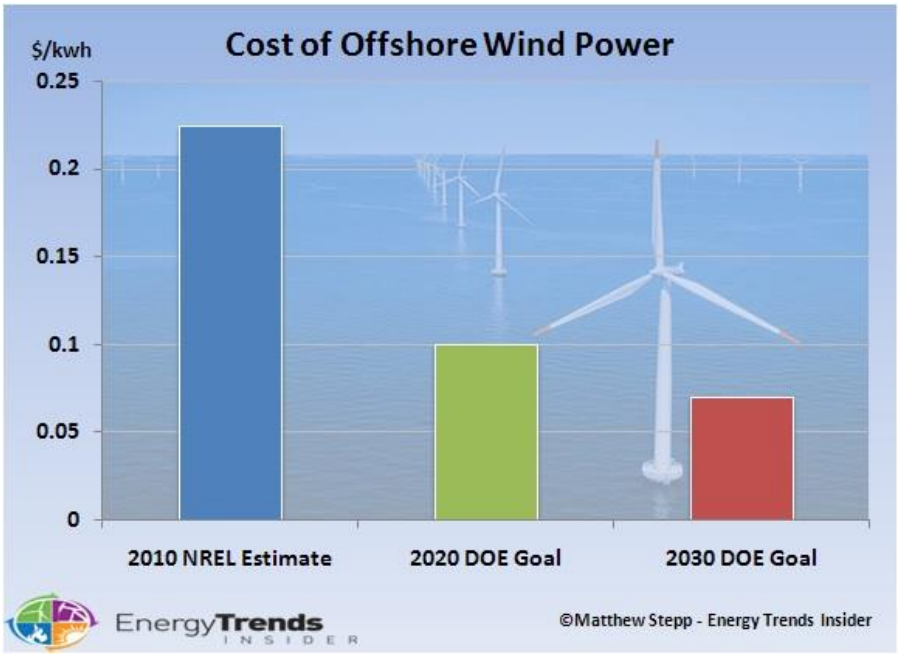

Figure 1 LCOE objectives for the next decades [4]

Given the tremendous growth potential of this young industry, investment will be required to understand some of the unknowns surrounding its installation and operation. As wind industry is an already mature industry, most of the concerns

now focus on what happens below the sea level, the supporting structure of the turbine. These uncertainties go from the design of the structure itself, to the O&M costs derived from the life of its components.

1.2 Supporting structures: State of the art

Depending on the seabed's depth and composition, there exist different alternatives for the wind turbine supporting structure. For example, floating structures are ideal for deeper seas, as building foundations big enough to connect the wind turbine with the sea bed would be costly as well as a technical challenge.

On the other hand, structures fixed to the seabed allow higher stability for the turbine, although they are limited to just a few geographical regions in the globe that gather the conditions of depth and wind quality. Among these structures, the most popular one is the monopole, accounting for over 80% of the offshore wind turbines in Europe [5]. Figure 2 shows a detailed sketch of a monopole foundation.

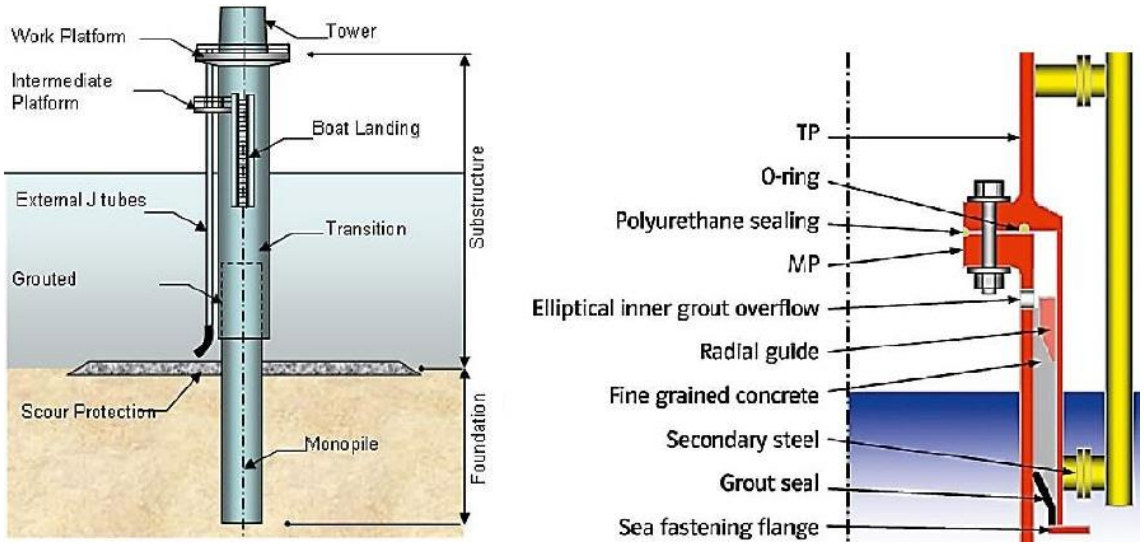

Figure 2 Grouted conection sketch

The connexion between the monopole and the wind turbine is achieved via a transition piece, which will be in charge of absorbing tolerances and inclinations of the system. It will as well simplify the installation process of the wind turbine

on top of the monopole. There exist two different techniques to join the transition piece and the monopole.

The initial practice was to generate a grouted connection, inserting one tube into the other and fixing them with concrete. However, this practice had not been thoroughly studied, especially in terms of long-term fatigue. Such is the case, that in 2010 it was found out that some of these connections were starting to fail, due to an initial underestimation of concrete failure, with a phenomenon called “ovalization” happening in the concrete connection. This was the result of a change in the shape of the concrete from circular to elliptic, making the transition piece more unstable, leading even to slippage. This deformation appeared because of oscillating momentum derived from horizontal cyclic loads from several sources: wind, waves, currents…

Considering that O&M costs in offshore wind turbines represent 30-35 % of the total cost, a reduction or elimination of one possible failure mode would result in a significant cut in the cost of electricity [6]. In order to achieve the aforementioned LCOE, a reduction of cost between 3 to 10 % is expected to come from substructure, cabling and substation costs [7].

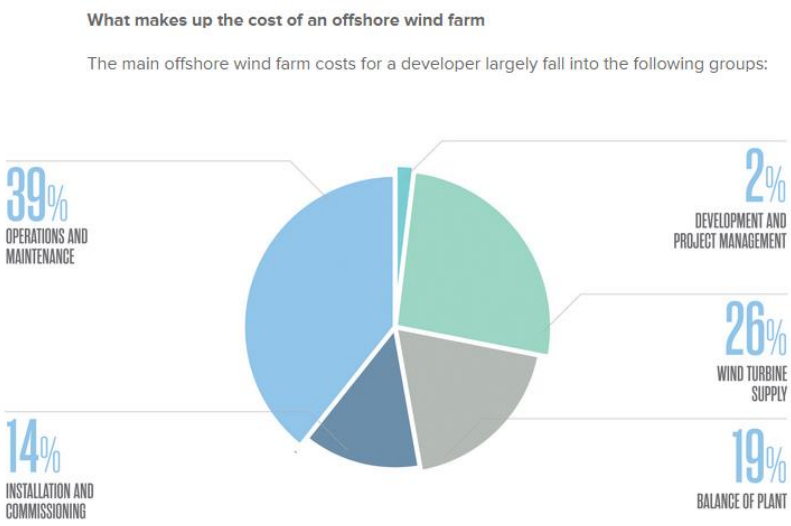

Figure 3 Offshore wind costs [8]

Regarding the second technique, some of the newest turbines are opting for a bolted connection using two flanges, one attached to the monopole and the other one to the transition piece. This type of connections have long been used in Oil and Gas industry, which is the main referent for the offshore wind industry. However, there are still some concerns surrounding this type of connections, due to the lack of existing research prior to the installation of the first wind turbines using this system. Topics such as bolt interaction, cyclic loading effects or short term relaxation are just some of the uncertainties surrounding it.

1.3 Scope of the project

Considering all the aforementioned information about the sector, the objective of the Thesis will be to develop a sensitivity analysis on some crucial issues surrounding M72 bolted connections. The first of them will consist in a comparison of the behaviour of the connection under different friction conditions, derived from the use or not of different coatings and/or lubricants. This analysis will focus just on the moment of application of the force, not considering any further effects due to external loading or short-term relaxation.

Following that research, a study on the possible effects of low temperature creep on the bolt will follow. This appears as an effort to model one possible cause of short-term relaxation in bolts using FEM software. The analysis will focus on the influence of creep on the bolt's tension field compared to the initial state, as well as developing a sensitivity analysis on creep parameters. Therefore, stablishing a guideline of which materials should be used in critical bolted connections such as these.

In order to do so, the first step will consist on giving some theoretical background about bolted connections of this size. This will include an analysis of the effects of considering the full scale of the problem, the selection of the load or the possible friction coefficients achievable in operation. In this first section some insight about low temperature creep will be given, alongside the equations used for this particular study. After that, the simulation environment will be described, based on real parameters for the geometry of both the flange and the connexion components (bolt, nut and washer). Some other properties will also be defined,

such as mechanical properties of the materials or friction properties; however these will be theoretical approximations, due to the lack of true experimental data prior to this test.

Finally, after the complete definition of the model, several simulations will be performed in order to determine any possible trend or relationship between the parameters modified and any operational condition surrounding the bolted connection.

2 LITERATURE REVIEW: BOLTED FLANGE CONNECTIONS

As it was introduced in the previous section, bolted flange connections are gaining popularity among the offshore wind sector, starting to replace concrete as the way to develop the transition from monopole to wind turbine. These connections use bolts (or studs), spaced uniformly along the flange, its number varying with the transition piece diameter, but also affected by the loads expected, thickness of the transition piece or bolt's size. The bolts will be preloaded in order to provide the required clamping between the two pieces, so that the quality of the connection can survive the expected operation time, under the loads specified and with minimum failure rates.

2.1 Theoretical background

The clamping force can be defined as the compressive force between the parts of the joint because of bolt tightening. This can be easily visualized with a spring model. Bolts are nothing else than springs that are pre-stretched and then fixed (by the nut), impeding any relative movement. The amount of tension achieved by the bolts is defined as preload. These "springs" will try to recover their natural length, generating a force directly related to the amount of stretch and the stiffness of the bolt's material.

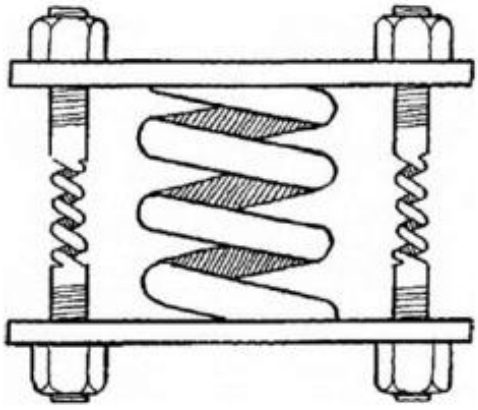

Figure 4 Flange's spring model

As a reaction of this compressive force, the flange will react as another spring, with, usually, a higher stiffness than the bolt, trying to recover its initial length. From this equilibrium in forces, appears what is defined as clamping force.

Several external loads affect bolted connections such as the one object to this study. Bolts, as springs, can be defined as energy storing devices, loaded with potential energy in the preload stage. This potential energy will be later affected by the aforementioned loads during operation [9].

2.2 Preload and influencing factors

The amount of preload that should be applied on the bolt depends on several factors. It needs to be high enough to provide sufficient clamping between the pieces connected, not only at the beginning, but also after this preload value has been affected by phenomena's such as relaxation, which will be later explained. If the clamping force does not reach a minimum value, the connection will loosen and increase the failure rates, not only in the transition piece, but also on the components placed over it, more affected by the cyclic loads acting upon the structure. However, on the other hand, an over-tightening of the bolt may lead to high stresses in the bolt or the nut, leading to abrupt failure, which will be catastrophic in most circumstances.

2.2.1 Bolt relaxation

Relaxation consists on a reduction of preload on the bolt that will consequently lead to a loss of clamping force in the flange. This phenomenon affects all bolted connections to some degree, and there are several parameters causing it. Some of them derive from long-term operation, caused by vibrations or cyclic loads, constituting the long-term relaxation. However, the present study will focus only in the initial stages after preloading the bolts, before external loads act upon the structure. This is a different category of relaxation, usually called short-term relaxation.

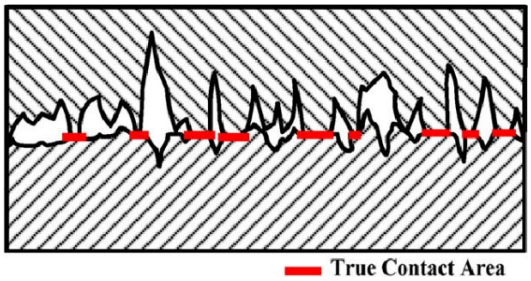

Figure 5 Imperfect contact surfaces

The main cause of this type of relaxation is early plastic deformation on some regions of the bolt, particularly in the thread or below the bolt's head. All these contact surfaces have some degree of imperfection, derived from the fabrication process. Because of these imperfections, the contact will not happen in the entirety of the surface, but only on a few points, as can be observed in figure 5. Because of this imperfect contact, the preload applied is distributed in only a few points instead of the whole surface, where tensions over yield stress (σ_Y) will appear. Hence, these contact points will deform plastically, until the contact surface increases, reducing these extremely high tensions. This plastic deformation will change the contact surfaces, smoothening the irregularities, in a process called embedment.

There are other factors that lead to short term relaxation, although with a smaller influence, such as short thread engagement, misalignment between bolt and hole or improper bolthole dimensioning [9].

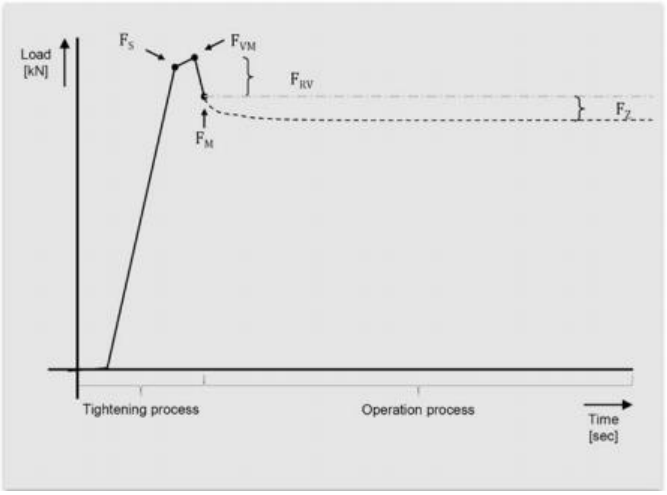

Figure 6 Visualization of short-term relaxation in tightening process

According to Kulak, Fisher and Struik in 1988, short term relaxation can produce a loss of preload of up to 11%, concentrated in the first hours, even seconds, after the application of the preload [10]. This can be seen in figure 6, where:

- F_S: Bolt load generated by tensioning cylinder
- F_{VM}: (Initial) assembly preload generated by tensioning cylinder and nut tightening
- F_{RV}= Loss of preload as a result of spring back (recovery loss)
- F_M= (Residual) assembly preload after releasing hydraulic pressure
- F_Z= Loss of preload as a result of embedding during operation
- F_{Mmax} = Maximum assembly preload
- F_{Mmin} = Minimum assembly preload

2.2.2 Pretensioning methods

The method used to tighten the bolt can as well affect the final preload of the bolt. There are several techniques for bolt tightening, being three the most popular: torque method, angle method and stretch method. The first two require a torque wrench to apply the preload on the bolt, whereas the third one uses a tensioning tool.

The first method is probably the most common method for bolt tightening. It applies preload by turning the nut around the bolt, increasing the load in the bolt until a predefined value of torque is reached. The formula relating torque and preload is:

$$T = KDF_{Pa} \qquad \textbf{Equation 1}$$

Where:

- T=torque (Nmm)
- K=nut factor (dimensionless), usually 0.2
- D=nominal diameter of the fasteners (mm)
- F_{Pa}=preload to be used at assembly (N)

The angle control method works in a similar way, using a torque wrench to repeatedly turn the bolt. This happens until a certain value of bolt stress is reached. From this point, the nut will be turned until a certain angle is reached,

instead of an amount of torque as in the previous method. One peculiarity of this method is that it usually goes beyond σ_Y (something that will not happen in the other two methods), trying to reduce the possible effects of embedment. This will reduce the difference between the expected and the actual preload [11].

Both methods, torque and angle control, have an advantage regarding the short-term relaxation effects. The process of rotating the nut and the bolt will happen with a certain amount of friction, which will smoothen the contact surfaces. These flatter surfaces will contribute to a reduction of bolt's short-term relaxation. On the other hand, the amount of torque being actually converted into preload is small, accounting only around 10% of the total torque applied, being the rest lost as friction in the thread region (40%) or in the flat contacts with the washers (50%). This will not only affect the amount of energy required to apply the same preload, but will also affect the scatter in the preload when using this method [11].

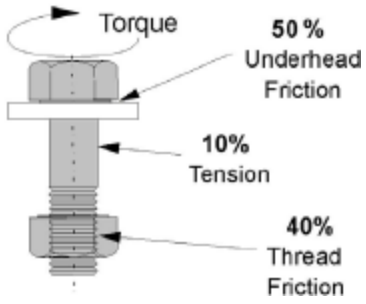

Figure 7 Torque distribution in the tightening process

The stretch method, unlike the previous two, uses a tensioning tool, instead of the torque wrench. The mechanic is quite simple, and it can be divided into two stages. The first one consists in pulling the bolt using a hydraulic system, generating the desired preload in the bolt shaft. Then, when that tension value has been reached, the nut us freely turned (manually or hydraulically), restraining the bolt, and not allowing it to return to its equilibrium position. This method is more efficient regarding the application of the preload; however, the amount of embedment will be higher than when using the other two methods, as torqueing process eliminates some of the imperfections in the contact surfaces. There exist techniques such as bolt training, which, in order to reduce imperfections in the bolt, turn the nut around the bolt before the actual preload is applied.

2.2.3 Tightening sequence and passes

In flanged connections, where several bolts are involved, the sequence in which bolts are tightened will also influence the final preload value. Tightening one bolt that stands next to a previously tightened bolt will affect its preload. Returning to the analogy of springs, the spring with high stiffness that was the flange, will be compressed further more when tightening the second bolt. This will consequently allow a reduction of the elongation of the previous spring or bolt, reducing its tension or actual preload.

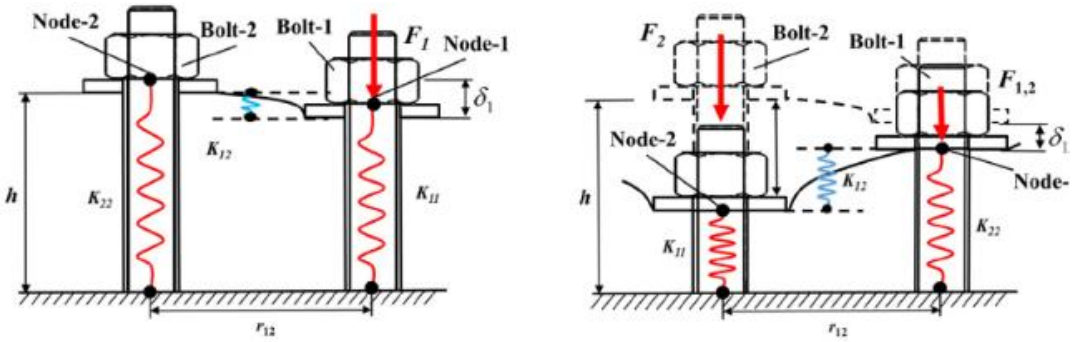

Figure 8 Visualization of elastic interaction

Ideally, if all bolts are tightened at the same time, this effect disappears, existing no elastic interaction between bolts. However, this is not practical nor cost effective. Therefore, industry has tried to develop certain tightening patterns that minimize the effect of neighbour bolts tightening. A common practice is to perform the star pattern, which reduces the elastic interaction and can be seen in figure 9.

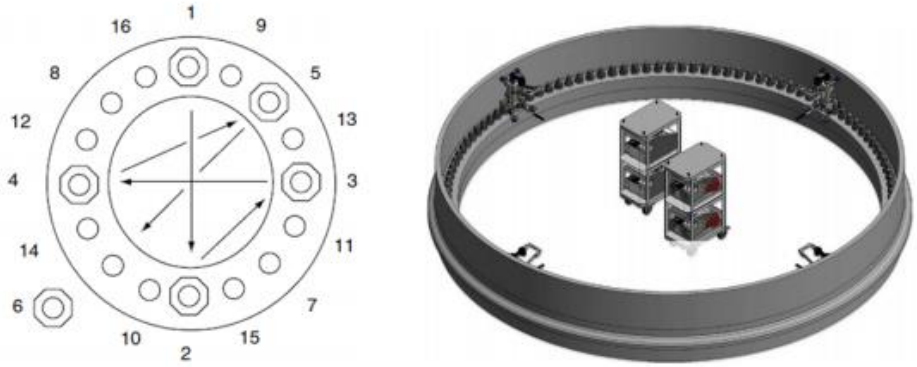

Figure 9 Usual bolt tightening pattern

A solution that stays in-between the previous two cases, would consist in defining a bolt-to-tensioner ratio configuration. That is, tightening all at the same time would require the same number of bolts and tensioners, 1 to 1 ratio. Manuals of bolt tensioning tools suggest that ratios of 1/2, 1/3 and 1/4 (50%, 33% and 25% at the same time) are also good solutions to minimise elastic effects and preload scatter, without requiring an excessive number of bolt tensioners [12].

The last option to minimize the preload scatter after tightening would be to apply the preload in separated steps. These steps allow some relaxation after the application of the load, although smaller, which can be partially compensated in the following step. These steps are called passes. The most popular number of passes is three, being five the maximum recommended. Figure 10 shows an example of a three pass bolt tightening. When using a certain bolt to tensioner ratio, it is also common to apply passes, equal to the number of divisions that have been made (1/3 ratio would require 3 passes).

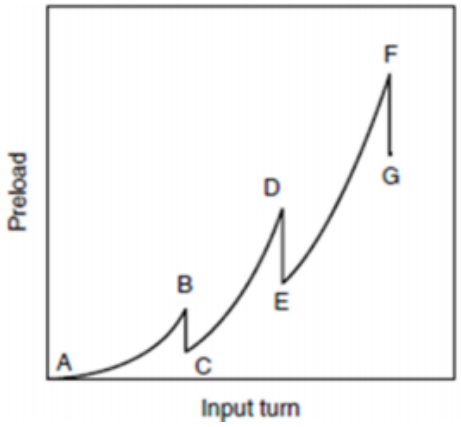

Figure 10 Example of three-pass tightening

2.2.4 Influence of bolt size

As mentioned in section 1, M72 bolts are the main objective of this study. This bolts, as well as the M64 bolts, are the most popular in wind industry [13]. These are bolts of remarkable dimensions, exceeding half a meter in length and 20 kilograms in weight, and therefore, not easy to handle in any experimental environment. However, scaled down tests are not possible, as respecting the original dimensions of the bolts is of paramount importance, for either designing

experiments or creating simulations. The reasons for this are the scaling effects in bolts, which are [14]:

- Geometric
- Technological
- Statistical
- Surface technological

The first one refers to the stress gradient in the bolt, going from the threaded external surface, with higher stress concentration factors that increase the tensions there, towards the less stresses centre. In higher diameter bolts, this gradient is smaller, existing therefore a bigger region affected by high stresses.

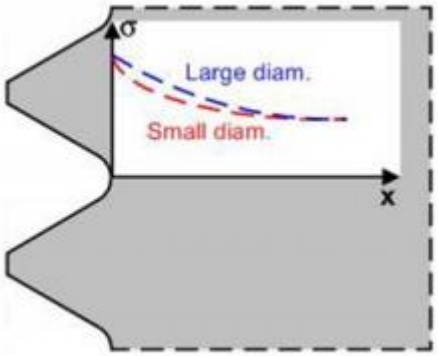

Figure 11 Visualization of geometric scaling effect

Both the technological and surface technological effects are manufacturing related. For example, a superficial treatment in a high diameter bolt affects a smaller amount of the bolt's volume when compared with a smaller bolt.

Finally the statistical size effect refers to the higher probability of getting imperfections or defects in oversized bolts [13].

These last three are relevant only when performing experiments, which is not the immediate aim of the present study. However, the geometrical size effect should be taken into account even when creating a FEM model, not to incur in initial misconceptions or errors.

2.3 Friction coefficients

In bolted connections, the friction coefficient (μ) is crucial, because if too low, it could lead to a loosening of the bolt. Usually, most producers recommend values in the range of μ=0.08 to μ=0.16, setting the minimum value at 0.04 [15]. Values of friction coefficients in bolts vary significantly, existing several researches showing different values and ranges of μ. It depends mostly on the type of treatment the bolt has suffered in the fabrication process, varying from one company to another. There are different techniques of bolt coating such as dip galvanization, electro galvanization...

Considering steel-to-steel contact, the most pessimistic predictions state a value for the coefficient of friction of up to μ=0.74, which could be even worse if these surfaces possessed some imperfections. However, considering bolts, most researches agree on values between μ=0.18 and μ=0.24. Then, using specific coatings could reduce it down to μ=*0.*11, and down to μ=0.08 if lubricants are used.

The coefficient of friction has a big impact, especially if torqueing tools are used, getting higher values of preload for a same torque the lower the friction coefficient. However, the influence of friction should not be neglected when using tensioning tools either, as it will be shown in the following sections of this research.

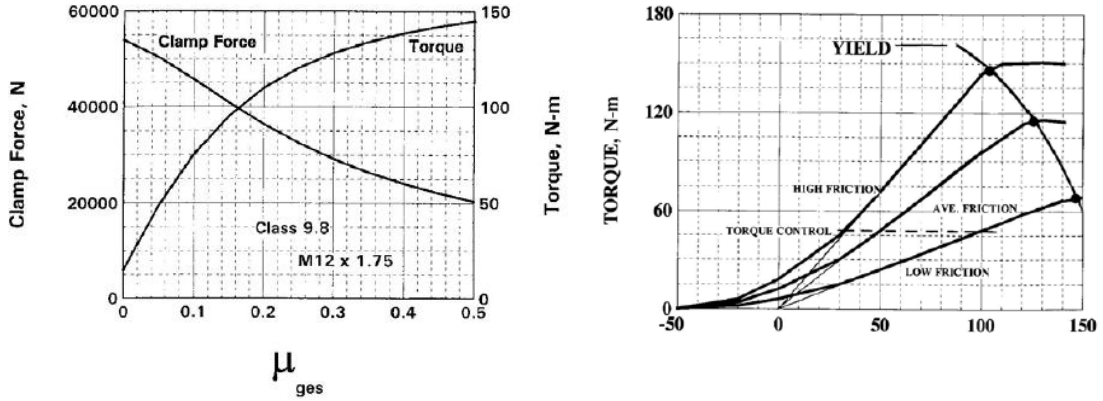

Figure 12 Evolution of (a)clamp and (b)torque with friction [11]

2.4 Low temperature creep

Several factors have been cited so far that lead to short-term relaxation. The most significant of them was the embedment, which is directly linked to material imperfections and roughness. Given the nature of this phenomenon, it is not possible to simulate it in a finite element model. Generating a rough surface would require infinite computational power, using microscopic element size in every contact surface, as well as creating a random pattern for the rough surfaces. Considering that the present model has several contact surfaces along the thread, the simulation of roughness is not feasible. [16]

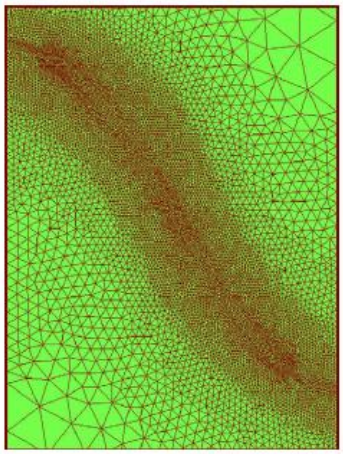

Figure 13 Example of meshing required to simulate rough surfaces

Therefore, this component of short-term relaxation should be tested via experimentation. The set of experiments that will try to quantify it are outside of the scope of the thesis, although will take place in the months after the completion of this document in Cranfield University Structural Integrity Lab.

However, there are some other relaxation sources that are not usually considered, but that could play a significant role in bolt's relaxation. Especially considering the magnitude of the loads acting upon it. One of these is creep. Usually creep is defined as a time dependent plasticity under a fixed stress and at elevated temperatures, which are usually over 0.5 times the melting temperature (T_F) of the material [17]. This phenomenon is studied at tensions bellow σ_Y, and is divided into three different phases: primary, secondary or steady state, and tertiary.

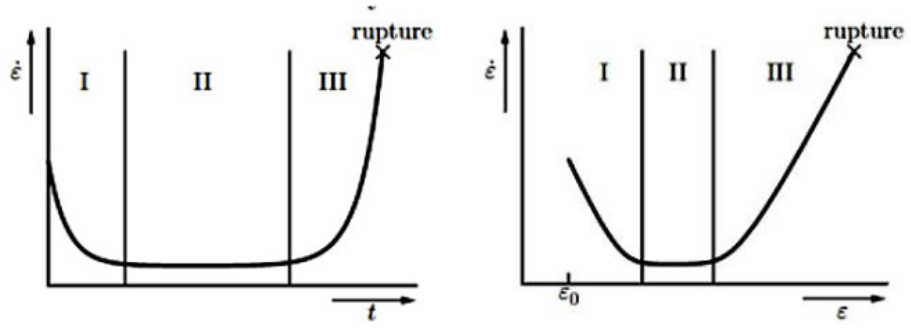

Figure 14 Examples of creep behaviour

Obviously, these are not the conditions present in normal operation in a wind turbine, where room temperature and loads close or over σ_Y (particularly in the thread region) exist. However, it has been found that creep at low temperature (LT) is still possible. The magnitude of it will be smaller; however, it might still be significant. Industry used to neglect it, but with the advances in measuring technologies, it is now being taken into account.

According to some research on high strength steel, similar to the one used in M72 bolts, even at tensions of 1/3 and 1/2 of σ_Y, there exists some creep deformation. However, the present study will focus on tensions over $0.9\sigma_Y$, as it will be explained in section 3. Appreciating the trend for the high strength steel (σ_Y=1250 MPa) in figure 15, it is reasonable to expect higher creep deformations at close-to-yield stresses [18].

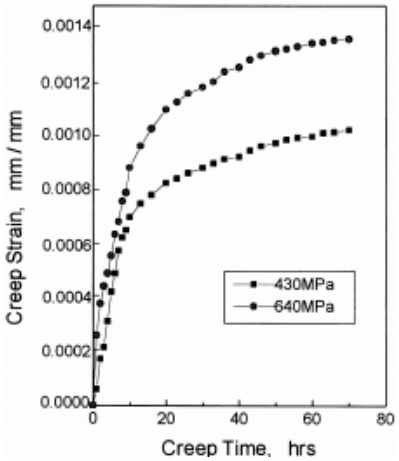

Figure 15 Creep strain curves of high strength steel

If the creep strain values in the bolt are big enough, they could directly influence the preload values on it, leading to a new source of relaxation that ought to be considered. This new relaxation would occur at the same time as the embedment, therefore the relaxation measured so far, accepted to be mostly caused by embedment, could as well be quantified in terms of creep.

2.5 Equations

2.5.1 Bolt preload

There are different theories on what value of preload should the bolt acquire in order to offer a service with guarantees, that is, maximizing the clamping force, but without exposing itself to plastic failure. All this theories are based on three parameters: material yield stress, cross section area and a safety factor.

$$F = cA_T S \qquad \textbf{Equation 2}$$

- F: Preload force
- c: safety factor
- A_T: Tensile shear area of the bolt
- S: Proof load of the bolt (usually 85% of σ_Y)

The value of c depends on the use the bolt will be given, using 0.75 for reusable bolts and 0.89 for one-use bolts. This factor is introduced as plasticity could appear in some particular regions of the bolt given the notches existing in the thread, which act as stress concentrators. Proof load is as well reduced to 85% to avoid plastic failure, although the original value of σ_Y can be used, too.

2.5.2 Ramberg-Osgood material model

Ramberg-Osgood material model is a simplified way to obtain a tensile curve for a material. It represents, not only the elastic region of the tensile curve, but also adds a second component representing the plastic behaviour of the material. The equation is as follows:

$$\varepsilon = \frac{\sigma}{E} + K(\frac{\sigma}{E})^n \qquad \textbf{Equation 3}$$

Being:

- ε: Strain
- σ: stress
- E: young modulus of the material
- K and n: material constants

Redefining it to fit the equation implemented in Abaqus software [19]:

$$\varepsilon = \frac{\sigma}{E} + \alpha \frac{\sigma}{E} (\frac{\sigma}{\sigma_Y})^n \qquad \textbf{Equation 4}$$

Being:

- σ_Y: Yield stress of the material
- α: Yield offset, which corresponds to $\alpha = K(\frac{\sigma_0}{E})^{n-1}$

2.5.3 Creep power law

There are several ways to define creep, however, the simplified power law will be the one used for the present study, as the lack of proper creep tests for the parameter definition would make it illogical to try a complex model. Creep power law can be defined as follows:

$$\dot{\varepsilon}_{cr} = A\sigma^n t^m \qquad \textbf{Equation 5}$$

Being A, n and m material and temperature dependent.

Of the three parameters conforming the set of uncertainties, the time component will be initially neglected by making m zero, resulting in:

$$\dot{\varepsilon}_{cr} = A\sigma^n \qquad \textbf{Equation 6}$$

This is because the worst-case scenario for the creep effects will be studied, assuming the initial (and maximum) creep strain rate as constant for a given tension throughout time, as the time period tested is a short one. However, as it will later be seen, the trend for high strength steels at low temperatures, is getting a reduction of creep strain rate with time because of work hardening (increment of dislocations inside the material), defined by that m constant, taking values between 0 and -1.

3 MATERIALS AND METHODS: MODEL DEVELOPMENT

In order to simulate the conditions as close to the real operation of the M72 bolts as possible, several steps were followed. First the generation of the geometries, those of the flange, bolt and nut. Then, the material properties of all the materials involved in the model. After that, definition of the contact properties, being this stage critical as the variation of the contacts is one of the scopes of the project. Finally, the application of the boundary conditions and the loads.

3.1 Geometry definition

3.1.1 Flange definition

The segment of flange designed is equivalent to a one-bolt partition of a 160 bolts flange. The dimensions of the original flange are shown in figure 16 [13]:

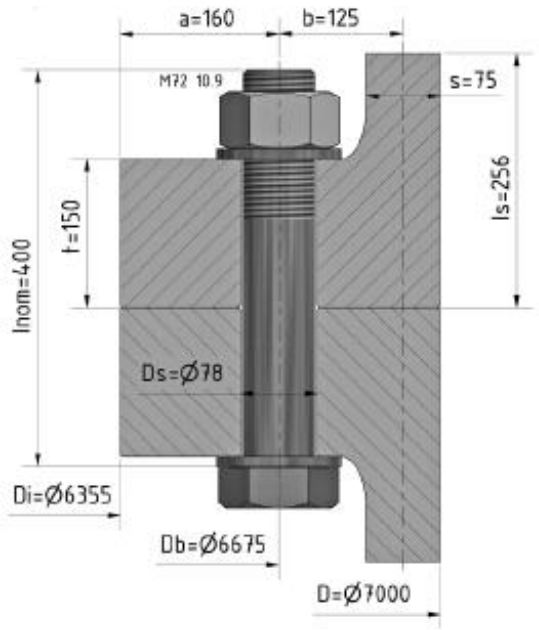

Figure 16 Flange dimensions

The total width has been calculated based on the diameter of the flange and the number of bolts in it. The angle between lateral walls has been respected (equivalent to 360/160 degrees). However, some other design details have not been considered, such as:

- The slope existing in this type of structures: Developing perfectly flat surfaces may lead into positive slope angles due to tolerances, which induce higher stresses than negative ones. Hence, some negative slope is preferred [20].
- The actual transition between the vertical and horizontal parts of the flange, manufactured in a forging process which introduces residual tensions, has been substituted by an R=5mm.

These simplifications were accepted, as they will not significantly affect the final state of tensions in the bolt, which is the object of study of the present thesis.

3.1.2 Bolt, nut and washer definition

The three elements where designed according to ISO4032 standards for M72 bolts. The detail of the dimensions can be seen in figure 17.

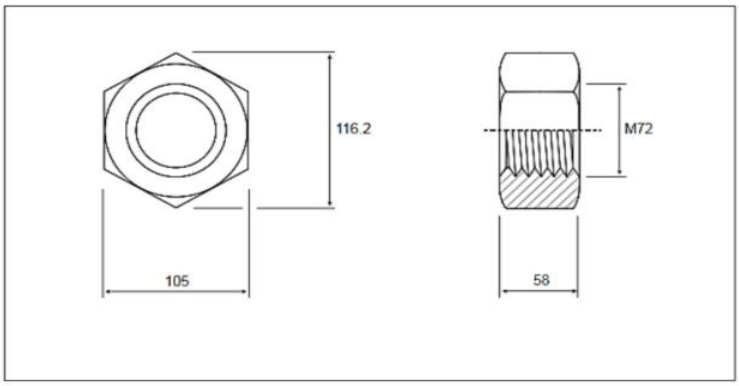

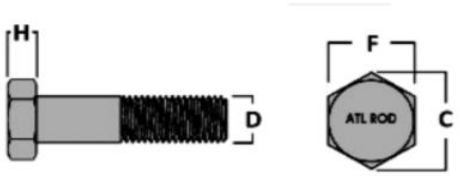

NOMINAL SIZE (D)	BODY DIAMETER	HEAD THICKNESS	ACROSS THE FLATS	ACROSS CORNERS	PITCH
	D (MAX)	H (MAX)	F (MAX)	C (MAX)	
M72	**72.00**	**46.45**	**105.00**	**121.24**	**4**

Figure 17 Bolt and nut dimensions

Maximum attention was given to the definition of the thread, as there is where most measurements will take place. The information about the thread, shown in figure 18, is based on a 4mm pith M72 bolt according to standards, having selected the minimum values within the range have been considered.

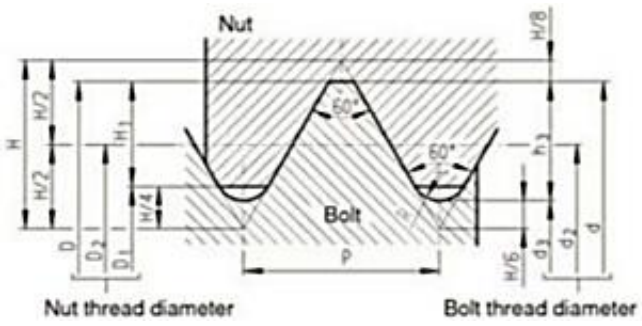

D_1 $d = 2H_1$
d_2 D_2 $d = 0.64952\ P$
d_3 $d = 1.22687\ P$
H $0.86603\ P$
H_1 $0.54127\ P$
h_3 $0.61343\ P$
R $\frac{H}{6}$ $0.14434\ P$

	External (bolt thread)							Internal (nut thread)							Basic mm
Pitch mm	Class	Major Dia d=D max.	Major Dia d=D min.	Pitch Dia d2=D2 max.	Pitch Dia d2=D2 min.	Minor Dia d3 max.	Minor Dia d3 min.	Class	Minor Dia D1 min.	Minor Dia D1 max.	Pitch Dia d2=D2 min.	Pitch Dia d2=D2 max.	Major Dia d=D min.	Major Dia d=D max.	Tap Drill
4	6g	71.94	71.47	69.34	69.11	67.61	66.642	6H	67.67	68.27	69.402	69.717	72	72.892	68

Figure 18 Thread dimensional definition

Some geometrical aspects that could affect the stress concentration factors in the bolt were not considered. One of them is the lack of fillet radius below the bolts head, that will introduce higher values of tension there than those that would exist in reality. Some other possible fillet radius in the sharp tips of the thread itself were not considered. They were neglected as they are not normalized, as they are a result of the fabrication process, and are quite small to be measured or meshed using Abaqus software.

3.2 Material definition

As it has been introduced, there will be two lines of research in this thesis. For the friction analysis of the bolt, only the instantaneous effects will be considered, without considering short-term relaxation effects. Therefore, a deformation plasticity model based on Ramberg-Osgood material model has been created. On the other hand, trying to consider the effects of short-term relaxation on the bolt, a research on the influence of low temperature creep effects will be made. Given the incompatibility of creep models and deformation plasticity, an elastic-plastic creep model was defined.

3.2.1 Deformation plasticity model

In the present model, there are three different materials involved:

- S355 structural steel for the flange (EN10025 standard)
- 27MnCrB5-2 grade stainless steel for the washer (EN 1.7182 standard)
- 10.9 grade high strength steel for bolt and nut (ASTEM A325 standard)

Given the lack of real tensile test data for all the materials, a simplified Ramberg-Osgood (RO) model was created to define the material behaviour.

3.2.1.1 Two point model vs multi point model

The ideal deformation plasticity model would be generated from a collection of data points obtained from a tensile test. These points, conveniently transformed from engineering to true stress values, would be adjusted using a minimum error criterion to the best combination of parameters of the RO equation for Abaqus (see equation 4).

However, there is only information available of s355 tensile tests. Therefore, other alternatives must be evaluated. Considering this, it is common to have information in the literature about two points of the tensile curve of materials, which are the yield point (usually according to the 0.2 % criteria) and the failure point (UTS). Given that the RO equation has only two unknowns (assuming E=210 GPa for steel), these two points could be enough to obtain a fit curve passing through them and through the origin.

To prove the quality of this method, an analysis of the available tensile test data for s355 steel has been performed. On one hand, a best-fit analysis to the tensile test has been performed in MATLAB, selecting the set of constants (α and n) that produced minimum cumulative relative error. This criterion was selected due to the non-uniform concentration of data points through the tensile curve.

$$error = \min\left[\sum abs(\sigma_{test} - \sigma_{RO}\Big)/\sigma_{test}\right] \qquad \textbf{\textit{Equation 7}}$$

On the other hand, selecting from the graph the yield and tensile points, the variables of the simplified RO have been obtained. Finally, another combination

of RO parameters was calculated based on literature data of the same material. In the following table, the different values of the parameters are shown:

Table 1 RO material model constants for S355 steel scenarios

	yield stress (MPa)	UTS (MPa)	UT strain(%)	α	n
RO multiple point fit	391.1	582.2	18.23	8.8	6.0
RO 3 point (tensile test)	391.1	582.2	18.23	1.04	11.3
RO 3 point (literature)	356.3	536.8	19.89	2.17	9.7

Figure 19 shows how the results are close to each other for the material, staying below 15% deviation in the worst position, with strains below 20%. There is an initial overestimation of stresses when using when using tensile test data for the three-point model. This is problematic as this is the range of strains more likely to exist in a flanged connection, where excessive strains are not plausible. However, the yield stress value obtained from the tensile test was of σ_Y=385 MPa, instead of the σ_Y=355 MPa obtained from the documentation, which slightly lowers the curve, improving the fit with the experimental results for strain values below 7%. Therefore, it can be accepted that the simplified three-point model is good enough for the material definition.

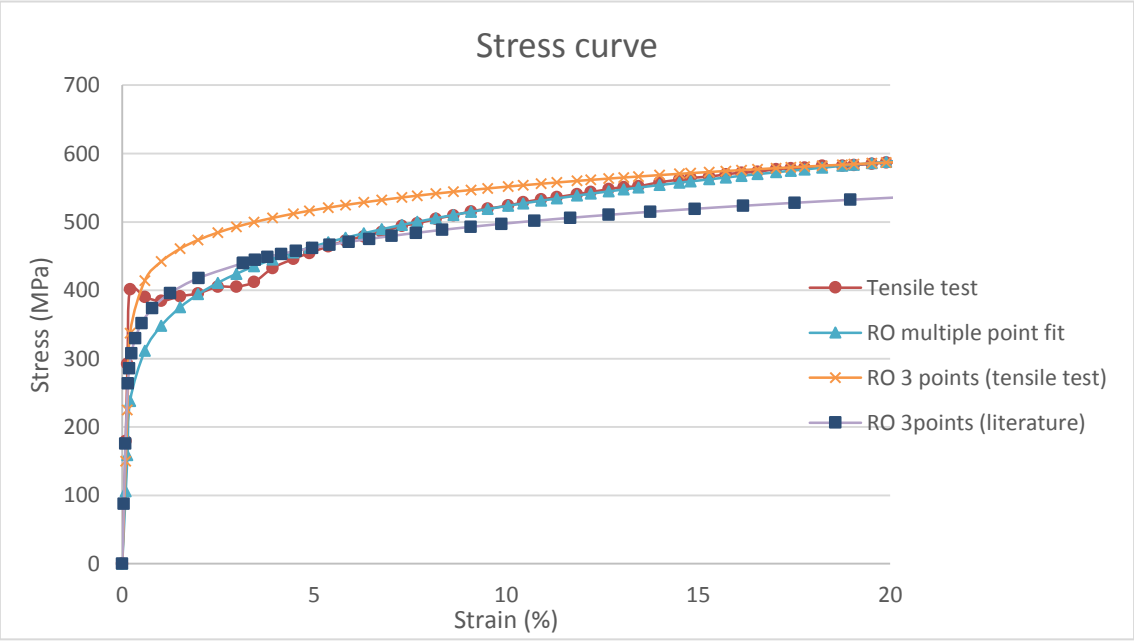

Figure 19 Different S355 stress-strain diagrams

Once the simplified model has been validated, the other materials can as well be defined, their properties shown in the table below. It has to be noted that the materials have been assumed isotropic, accepting the same elastic behaviour both for tensile and compressive efforts.

Table 2 RO material model constants

	Yield stress (MPa)	Uts min (MPa)	Uts strain (%)	α	n
S355	356.310119	536.8	19.89	2.17	9.7
27MnCrB5-2	754.1785714	1026	13.10	1.55	10.1
10.9 grade steel	946.087619	1133.6	8.62	1.43	14.0

3.2.2 Elastic-plastic creep model

The previously defined model was sufficiently accurate when studying the instantaneous application of the load. However, the second section of this project focuses on short-term relaxation due to creep in the first 48 hours after the application of the preload, which is the period in which LT creep is assumed to have the highest influence. Therefore, the deformation plasticity model cannot be applied on this scenario.

The phenomenon of LT creep, though rare and usually not significant in magnitude, can be considerable given the loads being applied, as it was explained in section 2.4. However, for the shake of simplicity, creep will only be considered in the bolt and the nut.

The creep behaviour will be modelled according to the simplistic power law creep model, which is determined by equation 5. In Abaqus software, this will be defined using time hardening creep property, setting the time constant m as zero.

As well as with the tensile tests, there is a lack of creep tests for this particular material, which is more acute when trying to find LT data. Hence, some other solutions will be needed. Tring to minimize the distortion that incorrect creep data might introduce in the model, tests under similar load conditions, low temperatures, and on mechanically similar materials have been used.

As a result of this, a study from the KTH in Sweden was used, which contains two different sets of information regarding high strength steels [21]. The first of them is a compilation of creep strain-rate tests of Bainite at 70 degrees Celsius. Despite bainite having a higher yield point than 10.9 grade steel (σ_Y=1600 MPa in the samples of their research), the temperature and the loads (around or over yield) are ideal.

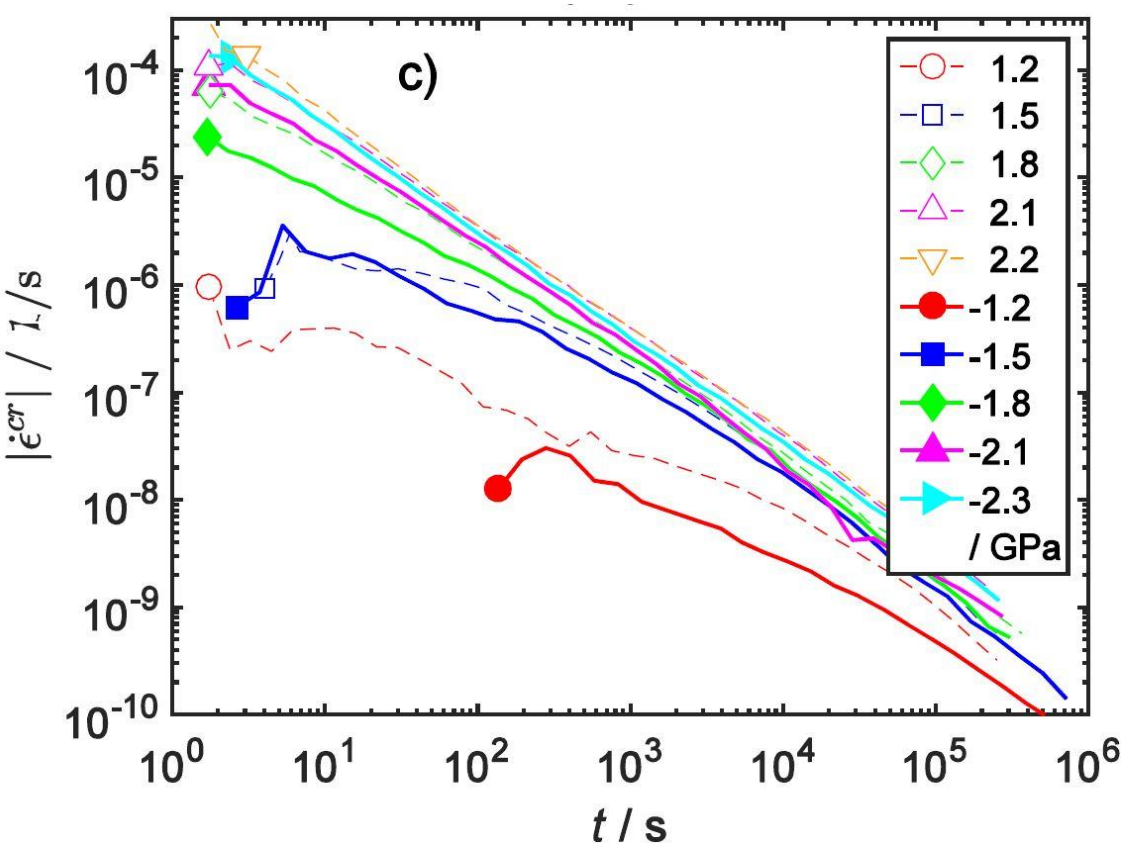

Figure 20 Creep tests from bainite at 70 ºC

On the other hand, the study focuses on martensite, material with a lower yield stress than that of the bolt (σ_Y=760 MPa), but also with several tests around yield tension values and low temperature. This is an interesting option as well, as the 10.9 grade steel has around 90% of martensitic structure, therefore its creep properties might be close to these [22].

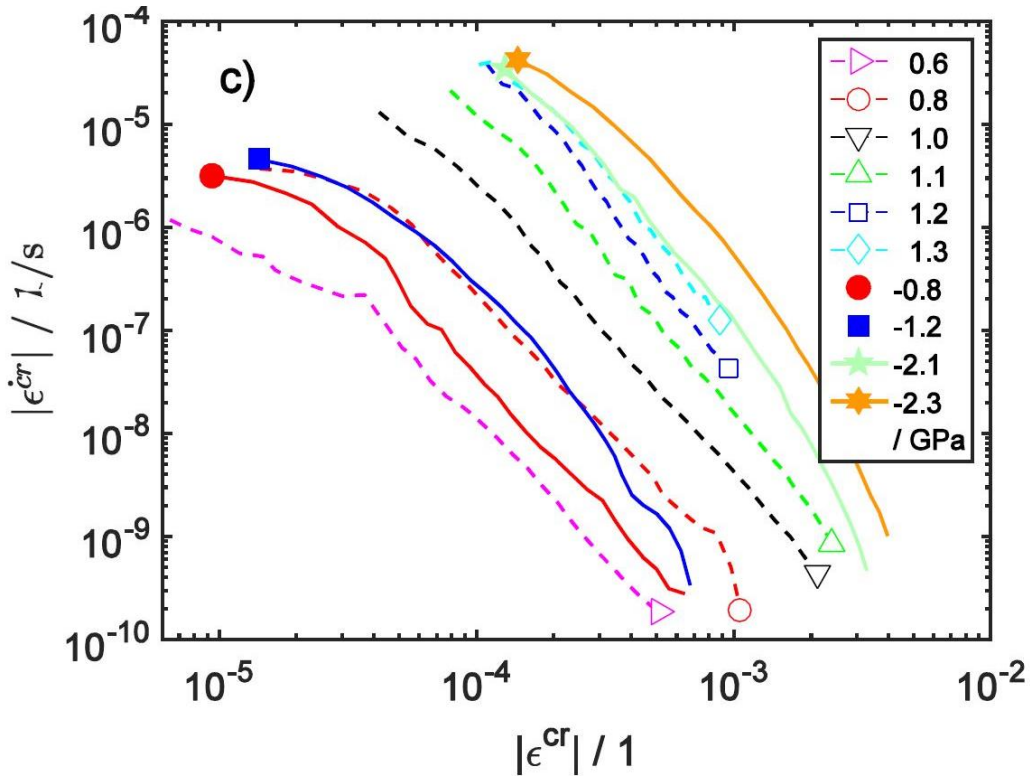

Figure 21 Creep tests from martensite at 70ºC

As explained in section 2.4, an assumption of time independency will be made, taking the initial creep strain rates at different tensions to develop the creep law. This will overestimate creep effects; however, it was considered a better option to assume the worst-case scenario for the present study. These values were fitted into the creep equation, in a procedure similar to that used for Ramberg-Osgood properties, with a minimum relative error criteria using MATLAB software.

Being both sets of constants designed for materials with higher (bainite) and lower (martensite) yield stresses than the bolt's material, some predictable trends will be seen. Using tensions below the σ_Y for results obtained around or over yield (the case when using bainite material model); will result in an underestimation of the creep strain rate ($\dot{\varepsilon}_{cr}$). On the other hand, tensions over yield stress (martensite) will result in $\dot{\varepsilon}_{cr}$ higher than expected.

Therefore, an intermediate material model has been created, trying to reach the best compromise between both materials. The *n* constant was obtained as an arithmetic average of the previous two, and the *A*, given the nature of the formula,

is the geometrical average of the original values. The final constants are shown in table 3.

Table 3 Creep constants for the three material scenarios

	A [h^{-1} MPa^{-n}]	n [-]
Bainite	3.532E-30	8.75
Martensite	1.820E-16	4.80
Combined	2.536E-23	6.77

These three different creep properties offer various scenarios of creep conditions for the simulations. Finally, plastic properties have been introduced based on the previously defined RO model, generating a set of points on the plastic region for the bolt and introducing them as an input in Abaqus software.

3.3 Contact definition

All the different contact surfaces forming the bolted flange connection have been divided into three groups.

- Flange to flange contact (FF contact)
- Thread to thread contact (TT contact)
- External contacts: horizontal contacts with the washers (EXT contact)

During the different simulations, each of these divisions will have a certain friction coefficient, depending on the conditions desired for the simulation.

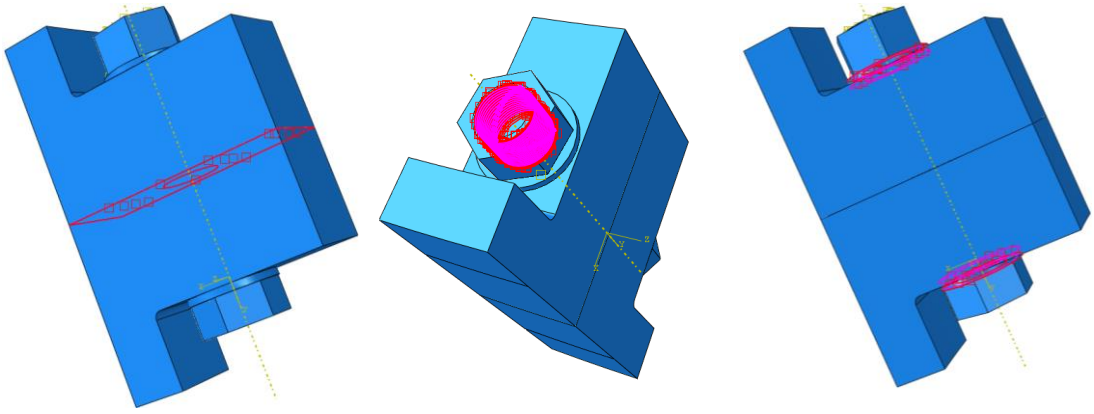

FF contact **TT contact** **EXT contact**

Figure 22 Models with the contact regions highlighted

As it was mentioned in section 2.3, there are several schools of thought regarding the value of μ for steel on steel. There are as well several combinations of coating and lubrication, each of them leading to a certain value for this coefficient. Therefore, two separated values within the range of possible coefficients have been selected, to perform a sensitivity analysis on friction coefficients, instead of focusing on a particular condition, which can only be precisely defined once the material is available for experimental testing.

Therefore, the values selected for μ are: 0.14, 0.25, 0.5 and 0.84. These friction values have been defined using the "Friction: Penalty" option in Abaqus in the contact surfaces previously selected. A general contact option was not possible given the different friction conditions acting simultaneously, in addition to the convergence problems that would be derived from its use in the threaded region.

The FF contact will be the same throughout all the simulations, assuming these surfaces as untreated, therefore with μ=0.84 values. On the other hand, the TT and the EXT contacts will vary creating various friction scenarios.

3.4 Load and boundary conditions definition

The whole system will be under the application of a simple set of loads. The first of them will be the gravity; however, the effect of weight (a total of 124 kg) is almost negligible. The second load is the bolt's preload (F). In bolts, F is based on three parameters, the cross section area of the bolt, a safety factor and the yield stress of the bolt's material, as shown in equation 2.

As it was mentioned in section 2, this paper precedes some experimental work that will take place in Cranfield University Structural Integrity Lab. One of the objectives of this research will be to evaluate the possibility of forcing the bolt closer to plasticity values, to see the effect this has on its relaxation. According to the experimental plan stablished by Cranfield University and Lic Energy for M72 bolts, a total preload of F=**2914 kN** will be used [23]**,** corresponding to a value close to 90% of σ_Y in the bolt. This is higher than the standard preload for this type of bolt, usually around F=2180 kN [24].

As the aforementioned experiment will apply the preload using tensioning tools, it has been assumed that the “Bolt load” command in Abaqus is close enough to the reality. Instead of developing the whole process (pulling-turning-releasing), which would involve more steps, hence a higher computational cost, the “Bolt load” option has been used. This method focuses on a middle section of the bolt, from which a portion of the bolt’s length will be subtracted. The amount of shortening will depend on the value of preload that is expected.

With this reduced bolt, keeping the rest of the assembly unchanged, the same load state as in real bolted connections is achieved, with the bolt working in traction, compressing or clamping the flange. In Figure 23, it can be seen how after the load application, around 2.1 mm of the central section of the bolt have been eliminated, resulting in a tensile state in the bolt.

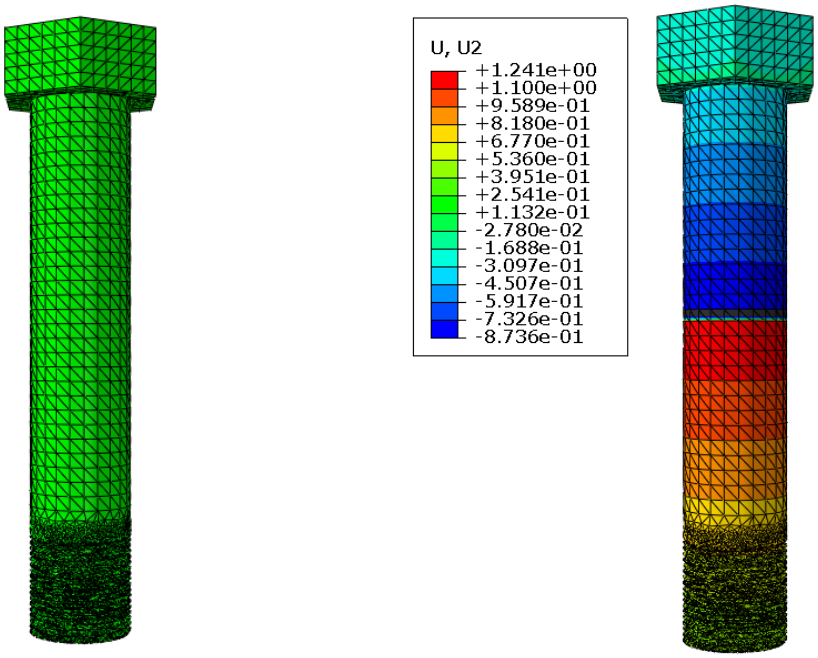

Figure 23 Bolt vertical displacement prior and after “Bolt load” application

In case short-term creep effects had to be checked, for the following steps the option “Fix at current length” for the bolt load has been selected. This option will allow bolt’s relaxation as some of the initial elongation of the bolt is reduced due to creep.

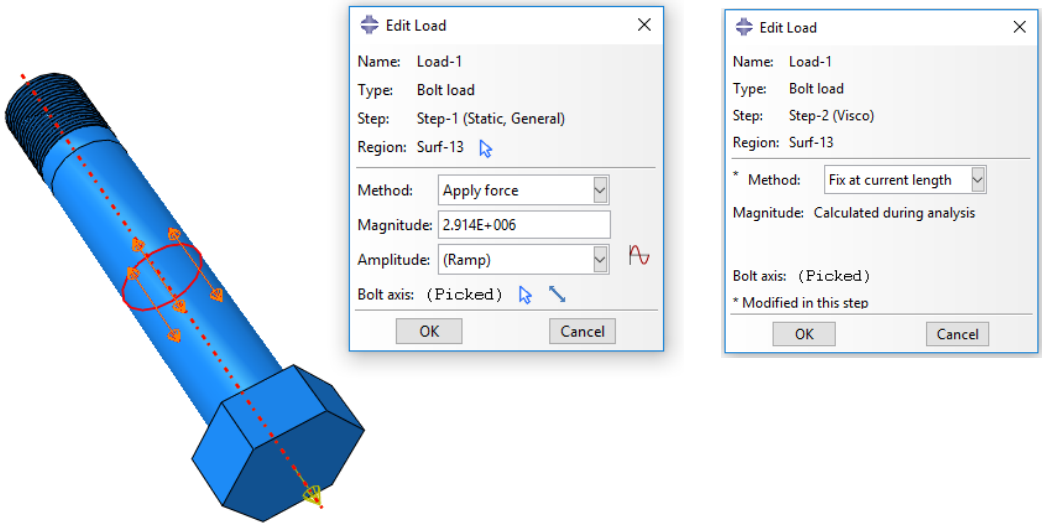

Figure 24 Details of the load applicattion

No other forces will be applied, as this study will not be considering relaxation due to external cyclic loading (long term).

Regarding the boundary conditions, trying to be as true to reality as possible, some considerations have been taken. The first is to encastre the lower surface of the flange, as a prolongation of the monopile used as a foundation in this wind turbine.

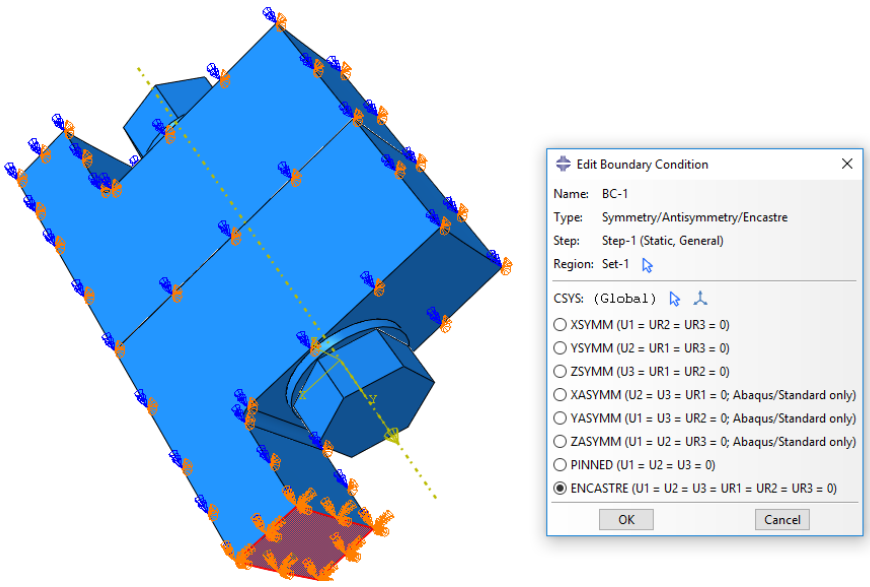

Figure 25 Bottom surface encastre

The other boundary condition for the system is to limit lateral movement in the flange, as this segment is in reality a small part of a bigger system, with each of the segments impeding movement to its neighbours. To simulate the presence of similar segments at both sides of this one, a symmetry condition was used.

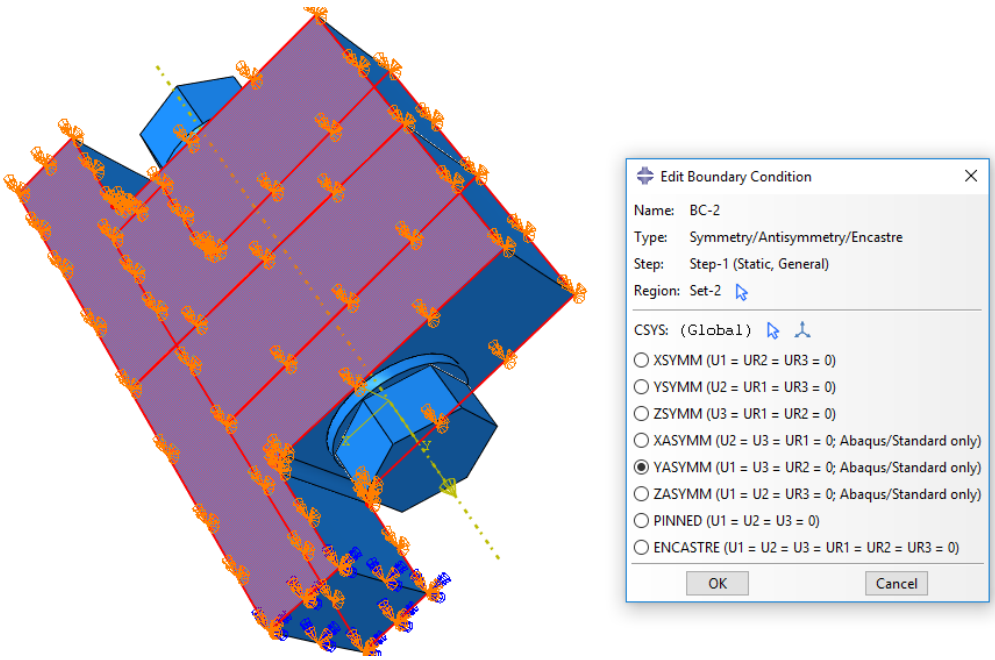

Figure 26 Symmetry conditions on the sides of the flange

Some other boundary conditions could have been used for the top part of the flange, as there will be a transition piece on top of it, causing some restrictions of movement. However, for simplicity reasons, they were not considered.

3.5 Mesh definition

Given the small dimensions of some of the details of the geometry, particularly in the threaded regions, special care should be taken while meshing. Several partitions were developed in the geometry to limit the total number of elements comprising the mesh, however it still resulted in a highly consuming mesh, that in addition to the number of contact points, make the system quite heavy computationally.

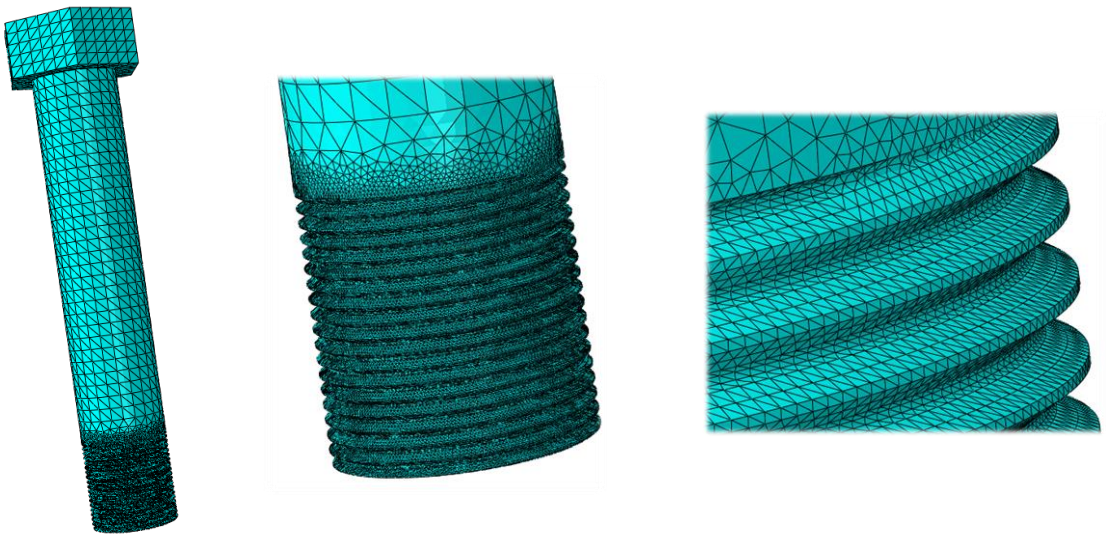

Figure 27 Detail of thread's mesh in the bolt

To avoid excessive element distortion in the thread, element size should be of 1 mm or less in the threaded regions. Therefore, these were the criteria for the meshing, limiting computational time but ensuring element quality was not exceeding reasonable limits regarding angles and aspect ratio. In addition, tetrahedral elements were selected due to their simplicity while meshing complex geometries. The washer was the only exception, formed by hexahedral elements.

After performing a mesh sensitivity analysis on mesh sizes of 4, 2, 1 and 0.5 mm, the final mesh has been selected. Its quality is reasonable, with only 0.05 % of bolt and nut elements with aspect ratios higher than 10, and below 0.1% exceeding the angular limits of 5 and 170 degrees,.

Table 4 Bolt and nut elements

Part: bolt	Part: nut
Tet elements: 253775	Tet elements: 194693
Min angle on Tri Faces < 5: 183 (0.072%)	Min angle on Tri Faces < 5: 79 (0.041%)
Max angle on Tri faces > 170: 35 (0.014%)	Max angle on Tri faces > 170: 2 (0.001%)
Aspect ratio > 10: 119 (0.047%)	Aspect ratio > 10: 92 (0.0473%)

In the following table it can be seen the total number of nodes and elements composing the mesh. In Appendix: Mesh, details of the different meshes are shown.

Table 5 Total mesh elements division

Total number of nodes: 851627
Total number of elements: 528930
527350 quadratic tetrahedral elements of type C3D10
1580 linear hexahedral elements of type C3D8R

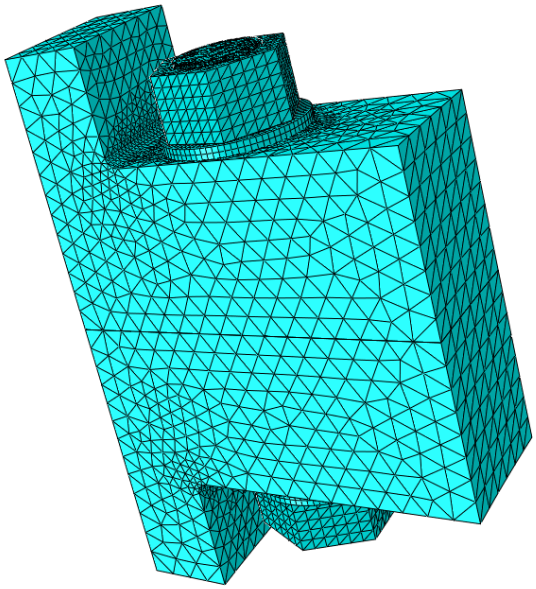

Figure 28 Final mesh of the model

4 RESULTS & DISCUSSION

4.1 Analysis of friction effects

In this stage a sensitivity analysis on the friction effects over the behaviour of the bolted connection will be performed. This friction will go from worst-case scenario steel-to-steel contact (μ=0.84) to an average lubricated surface (μ=0.14). Some intermediate values will as well be studied in order to obtain a better idea of the trends going on. There exist some previous analysis about this aspect; however they have focussed mostly in the variation of the preload. As it was already mentioned in section 3.3, the effects of thread friction and head friction will be analysed independently.

4.1.1 Data selection

In order to evaluate the possible effects of friction on the bolted connection, three different aspects from the model will be evaluated. The first of them will be the average tension of the contact surfaces of the thread. These are the most stressed points in the bolt; therefore, risk of plasticity will be higher there. Second, the contact pressure between the two flanges will be measured, which will represent the clamp achieved with the bolt applied preload. Finally, an individual analysis of thread tension will be performed, to determine if there is a correlation between friction and thread's tension depending on their position.

4.1.2 Thread friction analysis

For the first analysis, the friction coefficient in the thread (TT contact) will be changed to four different values, keeping the contact conditions in the remaining surfaces unchanged. To double check the results, two different frictions for the horizontal contacts (EXT contact) will be used. The aim of this step is to determine whether the TT friction affects the overall behaviour of the bolt, and, if that was the case, try to identify to which extent.

The first simulations have been performed assuming EXT contact as non-lubricated, that is a value of μ=0.84. This is equivalent to a no coated nor lubricated surface.

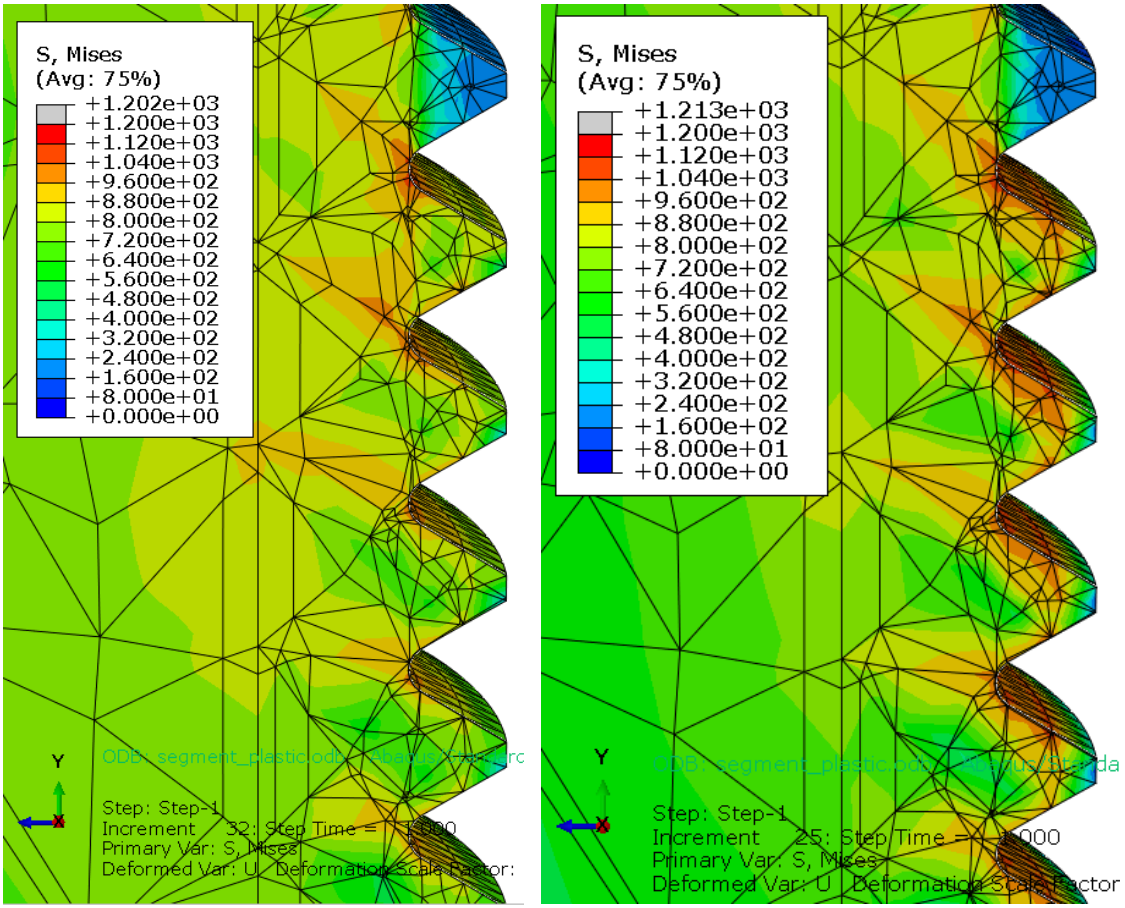

Figure 29 Threads 1-4. TT contact: 0.14 (left) and 0.84 (right)

Assuming a high friction contact in all surfaces excluding the thread, slightly lower values of tension in the system can be expected, as some of the energy is lost due to friction. The risk of corrosion would increase due to this lack of coating, especially in a harsh environment like the one in offshore facilities. However, a higher friction coefficient might contribute to reducing possible long term self-loosening in the bolt.

Figure 29 shows the contours for the Von Misses stress distribution in the initial threads under two different friction conditions. The tensional state inside the bolt is slightly higher when the friction is lower, as it was anticipated in the literature, and can be seen numerically in table 7. However, local values of tension in the contact points, are higher the higher the value of μ.

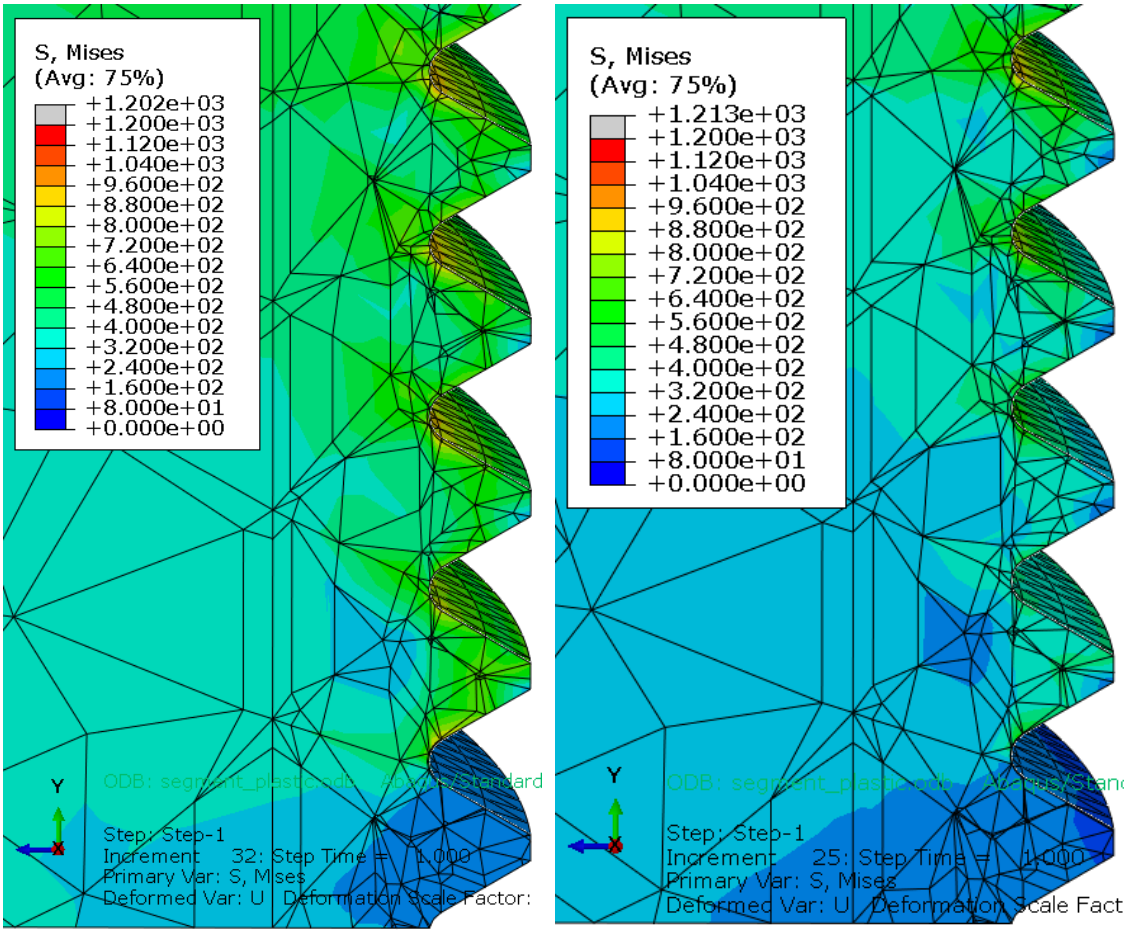

Figure 30 Threads 11-15. TT contact: 0.14 (left) and 0.84 (right)

On the other hand, figure 30 shows the final threads, comparing the same two values of μ fot the TT contacts. In this case, it is even more obvious how low frictions allow higher tensions in the bolt. In this case, not even the contact points reach higher tension values with higher friction coefficients.

Making an in depth analysis of the tensions in each thread, several points in each thread have been selected (belonging to both the valleys and the tooth of them). From this points, the average or maximum tension value for each thread have been calculated, from 1 (the first thread in contact with the nut starting to count from the washer side), to 15, being the first not engaged thread.

Evaluating the numerical results in figures 31 and 32, the first threads show higher stresses, values that diminish towards the end of the bolt. This was already known in industry, some even considering that, only the first three threads do

effective work. However, the most interesting result from the thread-by-thread analysis is that the level of engagement of the threads changes with friction. For example, a high μ contact will require slightly higher tensions to the first threads engaged, therefore increasing plasticity risks in those contact regions. On the other hand, this stresses fall more sharply towards the final threads. In other words, a contact with low value of μ will contribute to a better distribution of the mechanical load through the bolt.

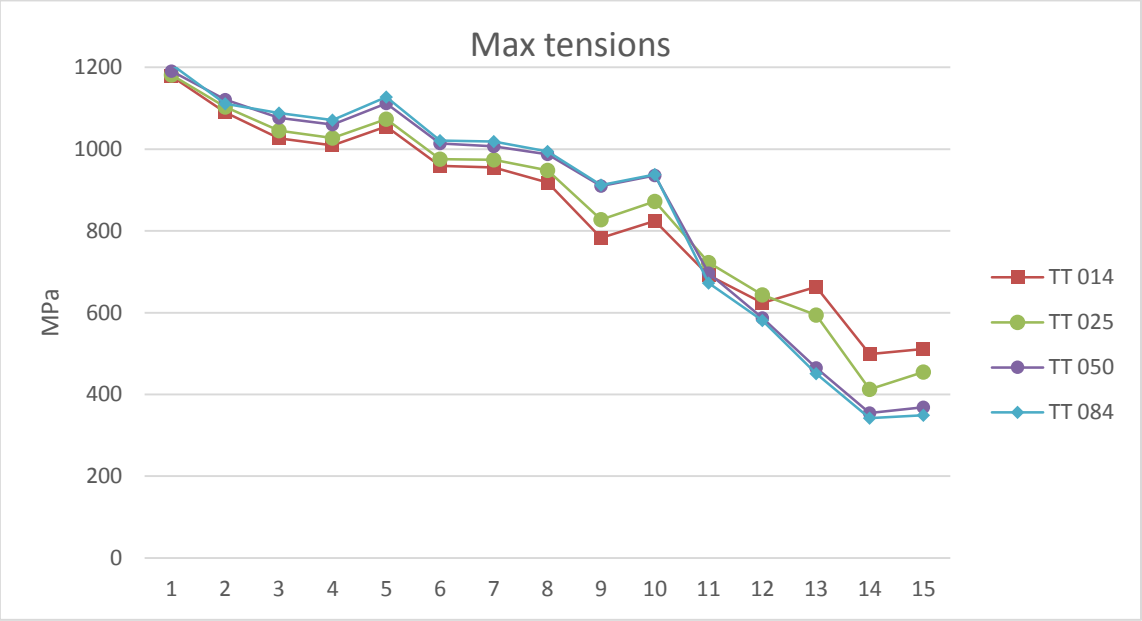

Figure 31 Maximum tensions per thread (EXT 0.84)

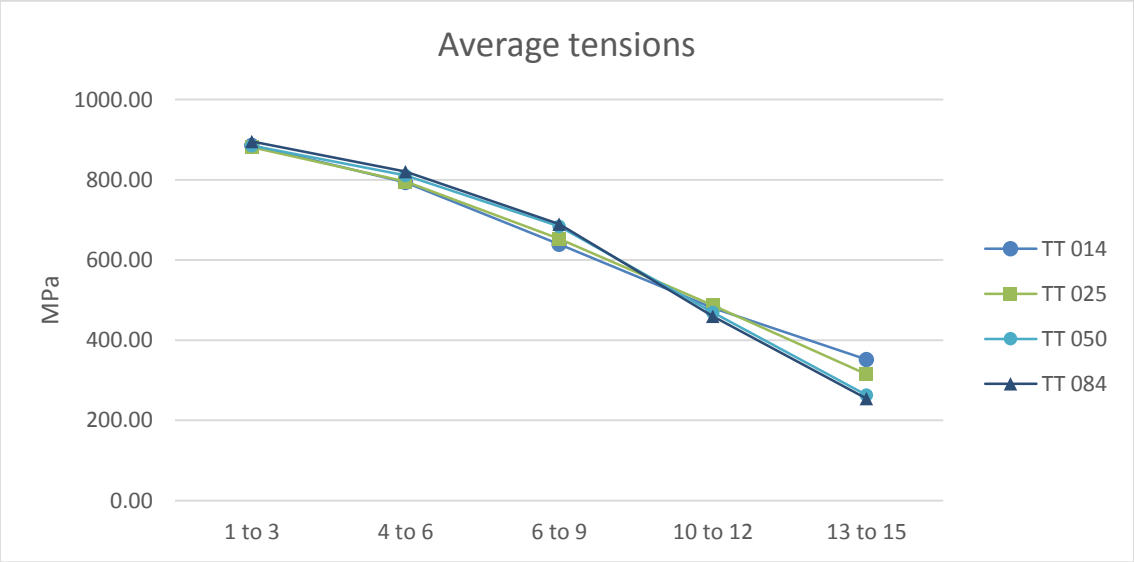

Figure 32 Average tensions every three threads (EXT 0.84)

This trend can be seen in both the maximum values per thread and the average ones. The figures show how tensions suffer an inversion around thread number 10, from which the stresses are higher the lower the friction.

The tensions in the thread are formed by a double tensional state, formed by the bolt preload or general tension, and by the contact pressures in the thread surfaces. The first component is higher the lower the friction, as it can be seen from the literature and observing the tensions inside the bolt. However, the first threads hide this, as contact pressures in those threads are quite significant, because these threads are the most active when talking about holding the bolt in place.

Therefore, assuming that plastic failure risk is directly related to maximum tensions, using better-lubricated contacts can reduce this risk up to a 3.5%, as shown in table 6. On the other hand, in the last few threads, after the inversion, there is no real risk of plastic deformation. Hence, having higher tensions there is indicating a more optimal use of the bolt and nut connection, by distributing the effort of holding the bolt in place in a higher number of active threads.

Trying to consider the effects that this will have on embedment and short-term relaxation, the same analysis can be made. High contact pressures are not interesting if short-term relaxation is to be reduced; therefore, lower coefficients of friction are preferred.

Table 6 Maximum tensions per thread group (EXT 0.84)

	TT 0.14	TT 0.25	TT 0.5	TT 0.84
1 to 3	1098.25	1.0%	2.9%	3.4%
4 to 6	1007.81	1.7%	5.4%	6.5%
6 to 9	885.47	3.5%	9.3%	10.1%
10 to 12	713.25	4.6%	3.7%	2.4%
13 to 15	557.37	-12.6%	-28.9%	-31.7%

Table 7 Average tension in the thread (EXT 0.84)

Average	TT 0.14	TT 0.25	TT 0.50	TT 0.84
Abs [Mpa]	630.12	626.25	622.59	623.92
Var (%)	xxxx	-0.6%	-1.2%	-1.0%

Repeating the same set of simulations for the thread friction, but this time considering μ=0.14 for the EXT, similar results are obtained. The analysis of thread tensions shows how the high frictions in the EXT surfaces were concealing the effect of varying the thread friction coefficient. The same trend appears, with better-lubricated threads providing a more uniform stress distribution along the threads, being slightly lower at initial threads, but with values higher for the final threads.

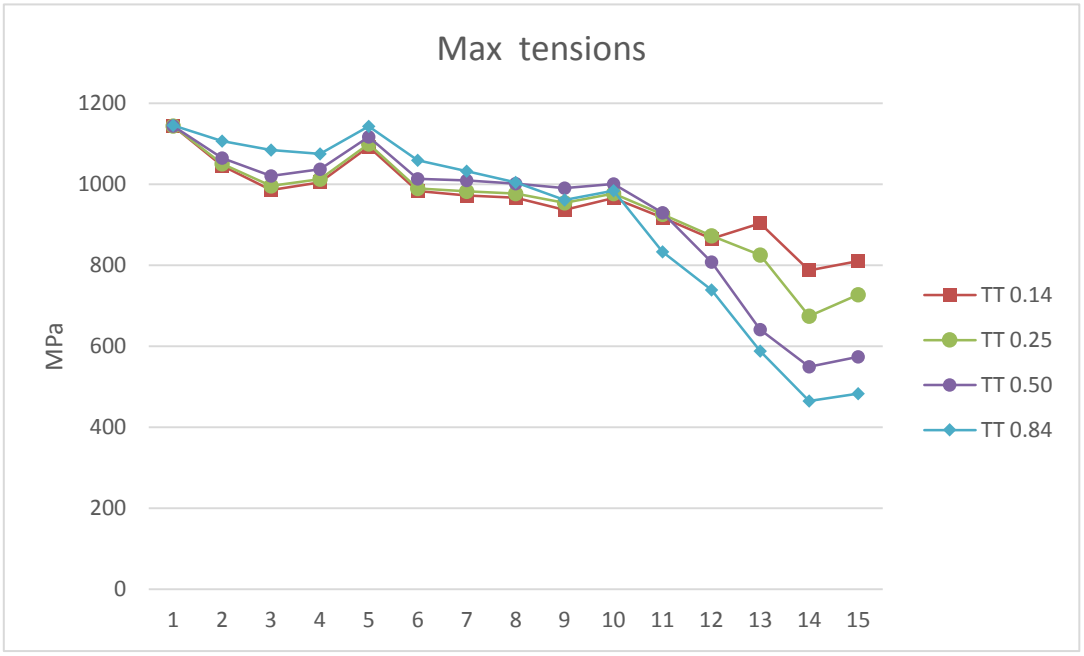

Figure 33 Maximum tensions per thread (EXT 0.14)

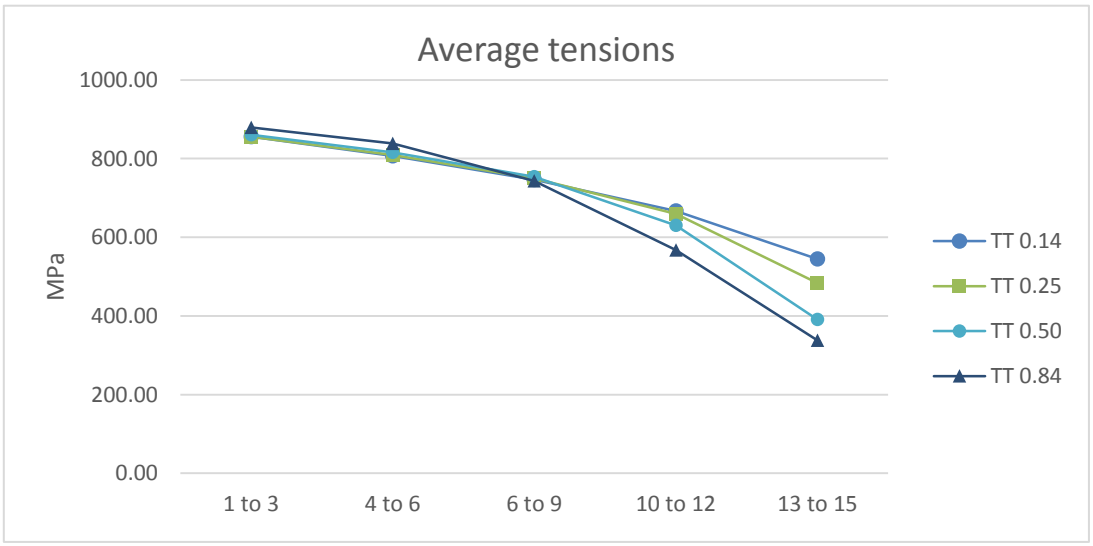

Figure 34 Maximum tensions every three threads (EXT 0.14)

This difference between the two scenarios can be better visualized showing the percentage variation of the values. In this case, comparing the results from tables 7 and 8, average thread tensions increase up to a 7 % when EXT friction is lower, compared to the almost negligible 1% from the μ=0.84 scenario, confirming that this high friction was hiding the effect of changing μ in TT contacts.

Table 8 Average tension in the thread (EXT 0.14)

Average	TT 0.14	TT 0.25	TT 0.5	TT 0.84
Abs [Mpa]	724.11	711.70	690.12	673.64
Var (%)	xxxx	-1.7%	-4.7%	-7.0%

Individual differences in each thread are also bigger, which can be seen in tables 6 and 9. They show how differences are increased, both for initial and final threads when compared to the μ=0.84 EXT scenario.

Table 9 Maximum tensions per thread group (EXT 0.14)

	TT 0.14	TT 0.25	TT 0.5	TT 0.84
1 to 3	1058.85	0.4%	1.7%	5.1%
4 to 6	1027.01	0.7%	2.8%	6.4%
6 to 9	958.55	1.3%	4.4%	4.3%
10 to 12	916.57	1.0%	-0.4%	-7.0%
13 to 15	833.86	-11.0%	-29.5%	-38.6%

Finally, evaluating the evolution of contact pressure in all scenarios, it shows that thread friction has no significant effect on the contact pressure between flanges, neither with lubricated nor with non-lubricated EXT contacts.

Table 10 Contact pressure between flanges (EXT 0.84)

Average	TT 0.14	TT 0.25	TT 0.5	TT 0.84
Abs [Mpa]	107.45	107.62	107.90	107.98
Var (%)	xxxx	0.2%	0.4%	0.5%

Table 11 Contact pressure between flanges (EXT 0.14)

Average	TT 0.14	TT 0.25	TT 0.5	TT 0.84
Abs [Mpa]	113.23	113.245	113.25	113.26
Var (%)	xxxxx	0.02%	0.02%	0.03%

4.1.3 General friction

For the second analysis, the friction coefficient in the TT contacts will be kept constant, changing the contact conditions in the EXT contact surfaces from lubricated to steel-to-steel contact. Again, to double check the results, two different values of μ for the TT regions will be used.

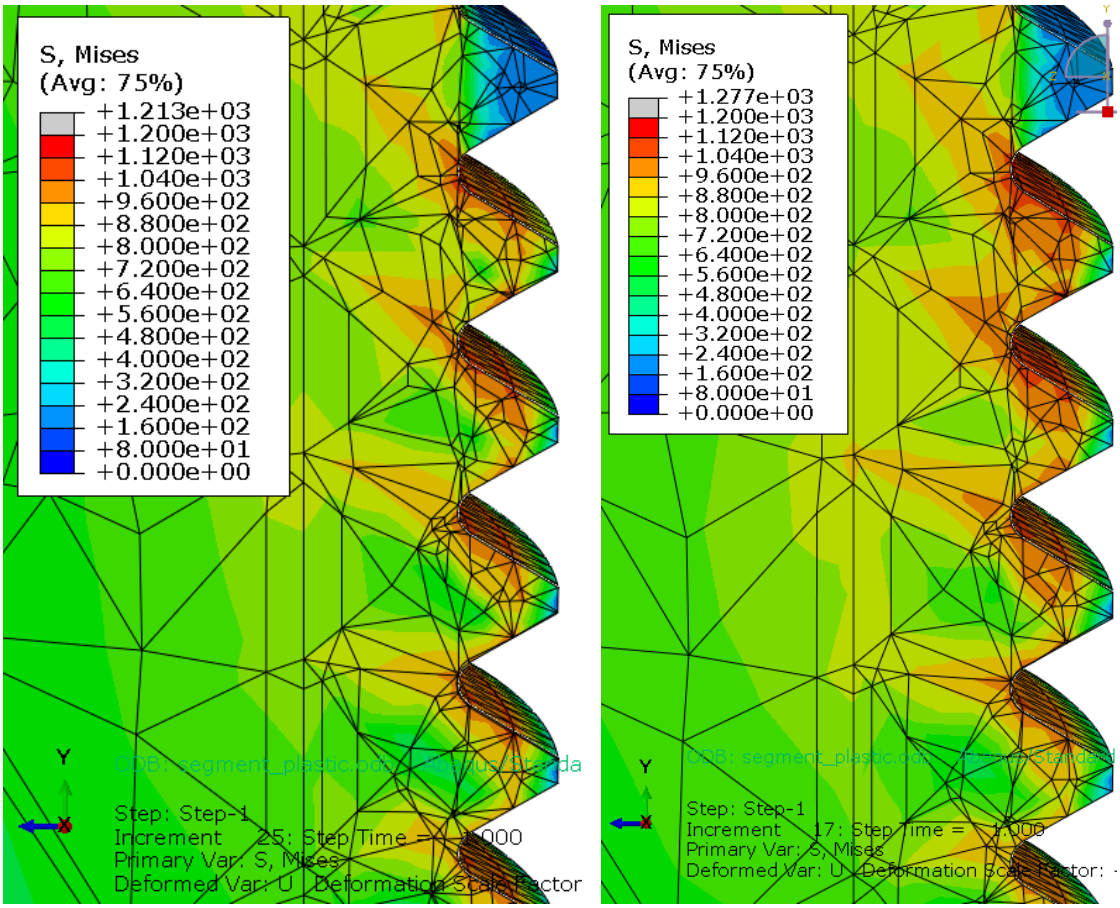

Figure 35 Threads 0-4. EXT contact: 0.14 (left) and 0.84 (right)

In this case, observing the contours from figures 35 and 36, they show how tension in the inside of the bolt are higher with lower friction coefficients. State that is more noticeable in the final threads. On the other hand, tensions in the surface are similar, given that TT value of μ is the same for both cases. However, there are slightly higher tensions around the valleys of the initial threads, caused by an increase in the overall friction of the system.

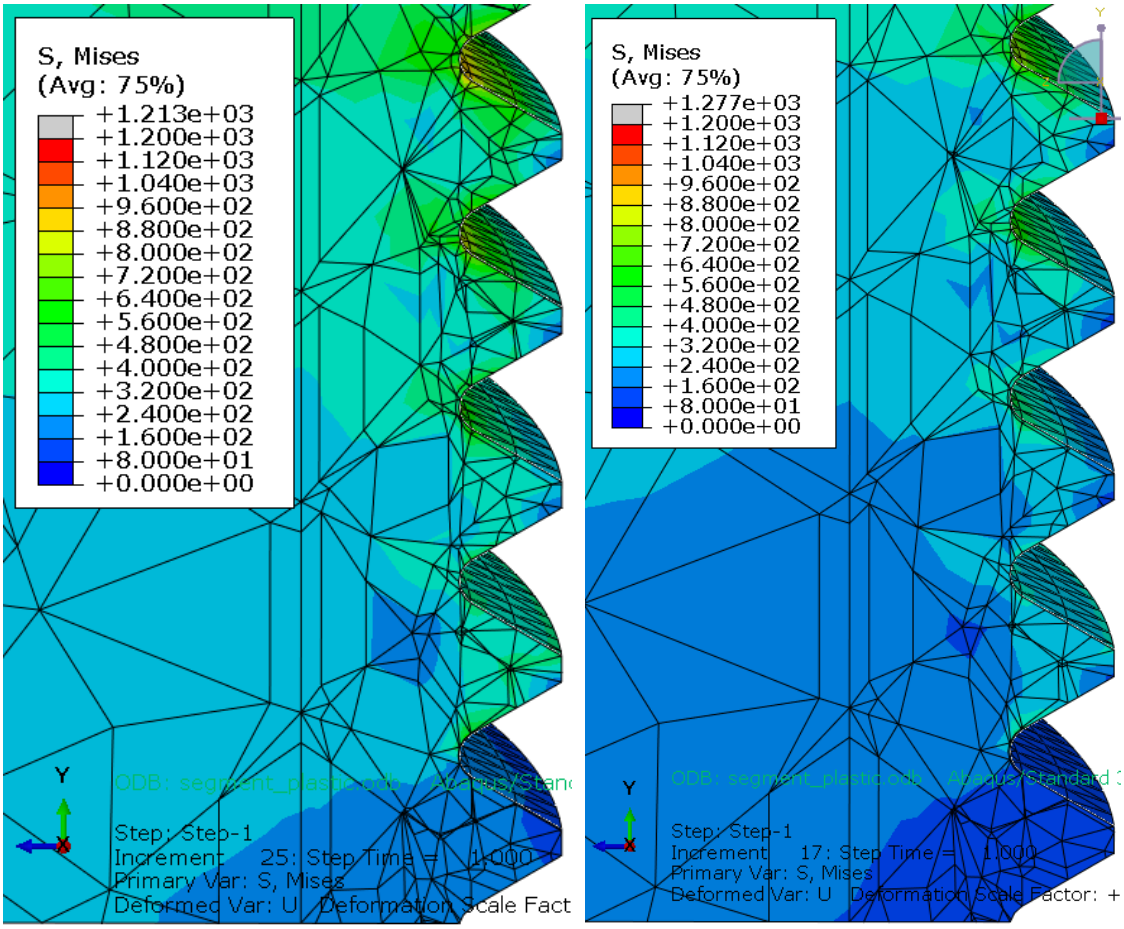

Figure 36 Threads 11-15. EXT contact: 0.14 (left) and 0.84 (right)

This change can be seen in the graphs from figures 37 and 38, which show a comparison of maximum values per thread for different μ in the EXT contacts, and for both TT scenarios. Tension distribution is better, especially at low TT frictions. Whereas low friction values for TT contacts were certainly positive regarding reducing plasticity risk, it is not that clear when talking about friction in EXT contacts. In this case, the change of tendency is happening earlier, in thread number four, where there are still tensions remarkably high that could pose risk of plastic deformation.

The increase of average tensions is quite significant when EXT friction is reduced. It is as well remarkable how TT values of μ=0.84 cause that sudden drop around thread 9, drop that disappears if this friction is reduced.

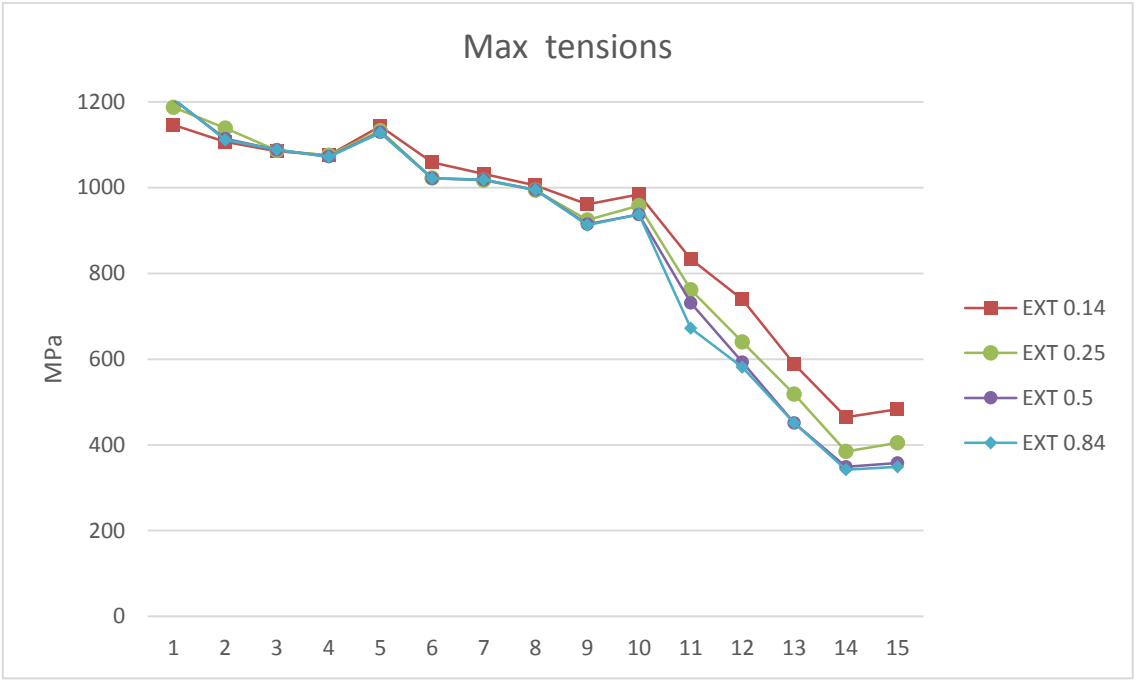

Figure 37 Maximum tensions per thread (TT 0.84)

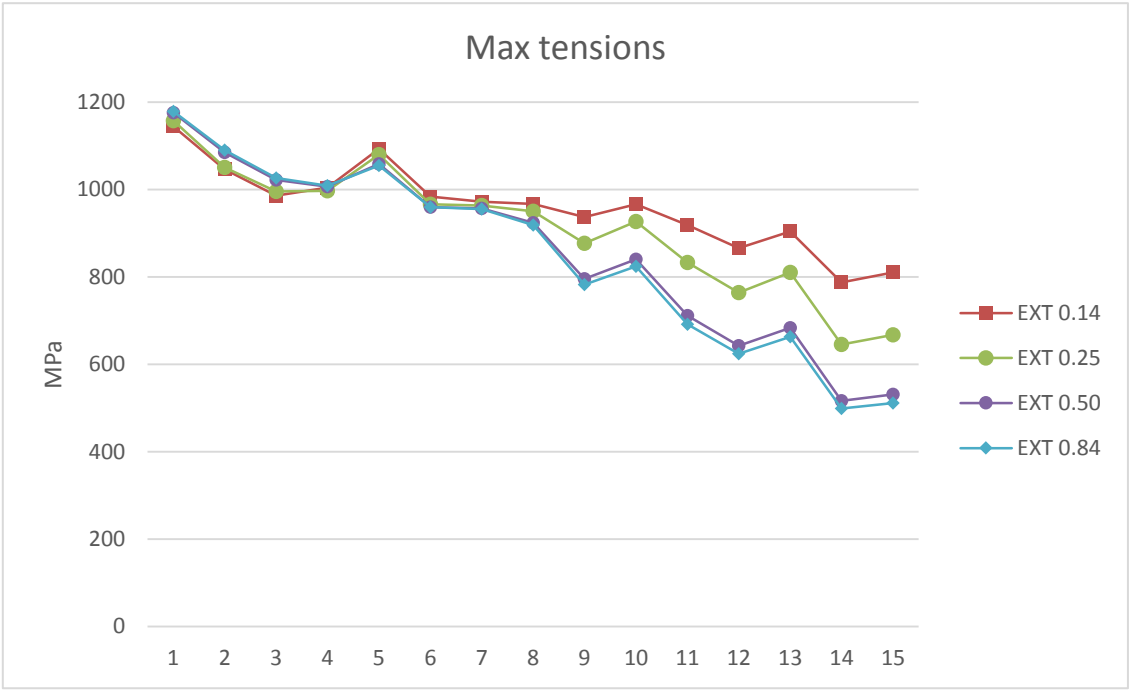

Figure 38 Maximum tensions per thread (TT 0.14)

As it was mentioned in section 4.1.2, as well as with the reduction of TT friction, reducing EXT friction also affects the average tension of the thread. This difference reaches 7.4% higher tensions with lubricated than with non-lubricated EXT contacts, as long as the TT contacts μ=0.84. When this value is reduced, the difference is even bigger, reaching 13%. It has to be noted, that when analysing the effect of changing thread friction, the maximum increment reached was only 7%. Therefore, it can be assumed that the friction coefficient around the washers is more determinant for the final tensional state.

Table 12 Average tension in the thread (TT 0.84)

Average	EXT 0.14	EXT 0.25	EXT 0.50	EXT 0.84
Abs [Mpa]	673.64	642.72	629.70	623.92
Var (%)	xxxx	-4.6%	-6.5%	-7.4%

Table 13 Average tension in the thread (TT 0.14)

Average	EXT 0.14	EXT 0.25	EXT 0.50	EXT 0.84
Abs [Mpa]	724.11	676.29	635.68	630.12
Var (%)	xxxx	-6.6%	-12.2%	-13.0%

Something similar can be said about contact pressure between the two flanges. It was pointed out in the previous section that they could be considered independent from the friction coefficients of the thread. However, observing the results from tables 14 and 15, there can be a difference of up to 5 % in the contact pressure between the flanges when having the EXT contacts properly lubricated, both in low and high friction TT scenarios.

Table 14 Contact pressure between flanges (TT 0.84)

Average	EXT 0.14	EXT 0.25	EXT 0.50	EXT 0.84
Abs [Mpa]	113.26	110.95	108.66	107.98
Var (%)	xxxx	-2.0%	-4.1%	-4.7%

Table 15 Contact pressure between flanges (TT 0.14)

Average	EXT 0.14	EXT 0.25	EXT 0.50	EXT 0.84
Abs [Mpa]	113.23	110.95	108.27	107.45
Var (%)	xxxx	-2.0%	-4.4%	-5.1%

4.1.4 Friction coefficients: discussion

After completing several simulations combining different friction coefficients for the different surfaces, it has been possible to determine and reach some conclusions. To begin with, the results obtained confirm that it is interesting to operate with low friction coefficients rather than with high ones. Some previous studies already suggested this result, as long as friction remained over a minimum value (usually over μ=0.05).

Usually these studies focus mostly on the final tensional state achieved in the bolt after applying a certain torque. However, friction does not only affect the tightening process. It can as well affect the overall tensional state of the thread. On this line, it has been proved that the factor influencing the most this final value is not thread friction, but the friction in the horizontal surfaces of bolt and nut, that is, the contacts on the washers, both with bolt and nut and with the flange. They exhibit a correlation by which highly lubricated surfaces offer a higher average tension in the bolt's thread.

This difference in average tensions in the thread can reach values of 13% when reducing EXT contacts friction coefficient. On the other hand, a variation on TT contacts friction of the same magnitude leads to a maximum 7% change. Therefore, friction in horizontal surfaces is more influencing than the friction in the thread itself regarding the total tensions of the thread. Lubricating horizontal surfaces will improve the transmission of preload to the bolt, and consequently the clamping force obtained in the joint. High friction coefficients will be inefficient, generating unnecessary energy losses in form of heat.

Further analysing the clamping force obtained in the different simulations, it can be seen how the contact pressure between the two flanges changes with friction too. Once again, it does not seem affected by TT friction changes. On the other hand, results show an increase of contact pressure with the decrease of μ in the EXT contacts, the same way the average thread tension did. In this case, the increase stays around a 5% difference between the two extreme scenarios of EXT friction. Therefore, clamping will improve with properly lubricated washers.

The second object of study of this friction research was not related to global behaviour, but with local tensions in the thread and the risks of obtaining plastic failure based on the friction coefficients used. Simulations have shown that the behaviour of each of the threads in the joint is not the same. There is a descending trend in tension, being the first threads, those closer to the flange, the ones under more stress. Bolt producers in the industry had already noticed this. However, this study has tried to analyse how this thread-by-thread reduction happens with the different friction coefficients.

From the graphs shown in sections 4.1.2 and 4.1.3, both TT and EXT friction coefficients affect the way thread-by-thread tension changes. With low friction coefficients, the superficial tension in the contact points of the initial threads is slightly smaller than with higher friction coefficients. Given the nature of bolted connection, these tensions will diminish the farther they are from the flange. However, high friction coefficients make this transition abruptly, while on the other hand, better-lubricated contacts offer a smoother transition. This is interesting as it means that low friction contacts contribute to a more efficient work distribution through the thread, with more activity from threads that would be “inactive” if frictions where higher. It is as well important to note that higher tensions in the initial threads, even if the difference is small, will lead to an increase in the likelihood of plastic failure in those regions.

Hence, it can be concluded that low friction coefficients will positively contribute to bolt operation. First, the transmission of tensions will be better, obtaining more preload in the bolt with the application of the same amount of energy (whether with the torque or tension method). Second, achieving proper lubrication in the washers, will improve the clamping force obtained with the tightening of the bolt. Finally, risk of plastic deformation will be reduced, thanks to a better distribution of preloads along the threads, instead of concentrating most efforts in the initial threads.

4.2 ANALYSIS OF LOW TEMPERATURE CREEP

As it was mentioned in section 2.4, some simulations analysing the effects of low temperature creep on the bolted connection will be performed. These will try to prove the influence of creep at low temperatures with loads that go beyond yield stress in short 48 hour periods. During this time, the loading and friction conditions will not change.

4.2.1 Material creep comparison

As it was mentioned in 3.2.2, different creep properties will be simulated, for materials with lower and higher yield stress than that of the bolt, which should, respectively lead to high and low values of creep. The third model consists in an average case based on the other two that is expected to be closer to reality.

The three models have been created for conditions of 70 degree Celsius, and assuming that the initial (and maximum) strain rate of the material applies for the 48-hour period. This is obviously an overestimation, but the main purpose of this section is not finding the exact value of creep, but determining if its effect on relaxation should be neglected, and if not, perform a sensitivity analysis afterwards.

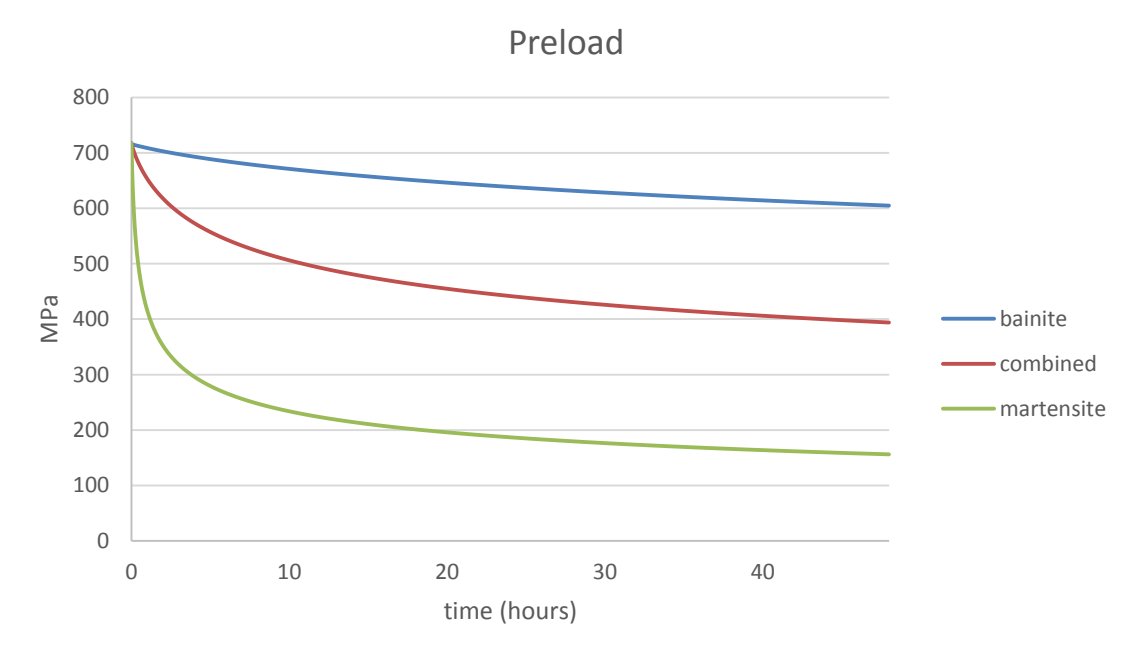

Figure 39 Preload relaxation after 48-hour period

In order to evaluate the results, the evolution of the average tension at the middle of the shaft of the bolt has been measured. Figure 39 shows how the power law creep introduced affects the final tensional state of the bolt, reducing its eeffective preload, and consequently the clamping force exerted on the flange. Observing the three different materials considered, it is obvious how softer materials (martensite), lead to higher relaxations. This is because of the fact that, comparatively, tensions in the bolt are higher for martensite than for bainite, with the tensions reaching values close to 1.5 times martensite's σ_Y. Another reason could be the definition of the creep law itself. Martensite and bainite power laws were generated for a range of tensions around yield. Hence, considering tensions inside or outside those intervals might affect the results. In the following table, the total relaxation after a 48-hour period can be seen.

Table 16 Amount of relaxation depending on the material

	Preload (0h)	Preload (48 h)	Loss (%)	Ratio
bainite	717.12	604.74	16%	1.00
combined	717.12	416.30	42%	2.68
martensite	717.12	156.14	78%	4.99

Figure 40 shows the evolution of the contact pressure between the two flanges, as well as the total energy dissipated by means of creep, showed in figure 41. It is easy to notice how the profile of the creep dissipation, bolt preload and contact pressure is similar, as they are directly interrelated. The three of them show a logarithmic shape, which should stabilize around a certain value if enough timeis given. The lower the σ_Y of the material used to define the creep model, the faster it stabilishes. On the other hand, bainite's creep model seems to need longer to reach that equilibrium.

Even with the time component eliminated from the equation, there is still some time dependency. This is caused by the relationship between bolt's length and bolt's preload. Initially, creep rate ($\dot{\varepsilon}_{cr}$) should be constant at each point and tension, which would lead to a straight creep strain curve. However, with a certain amount of creep strain, bolt's length increases, reducing the clamping in the flange, relaxing. Hence, it is this reduction of tensions in the system that reduces $\dot{\varepsilon}_{cr}$ with time, even when time hardening is not considered in the creep models.

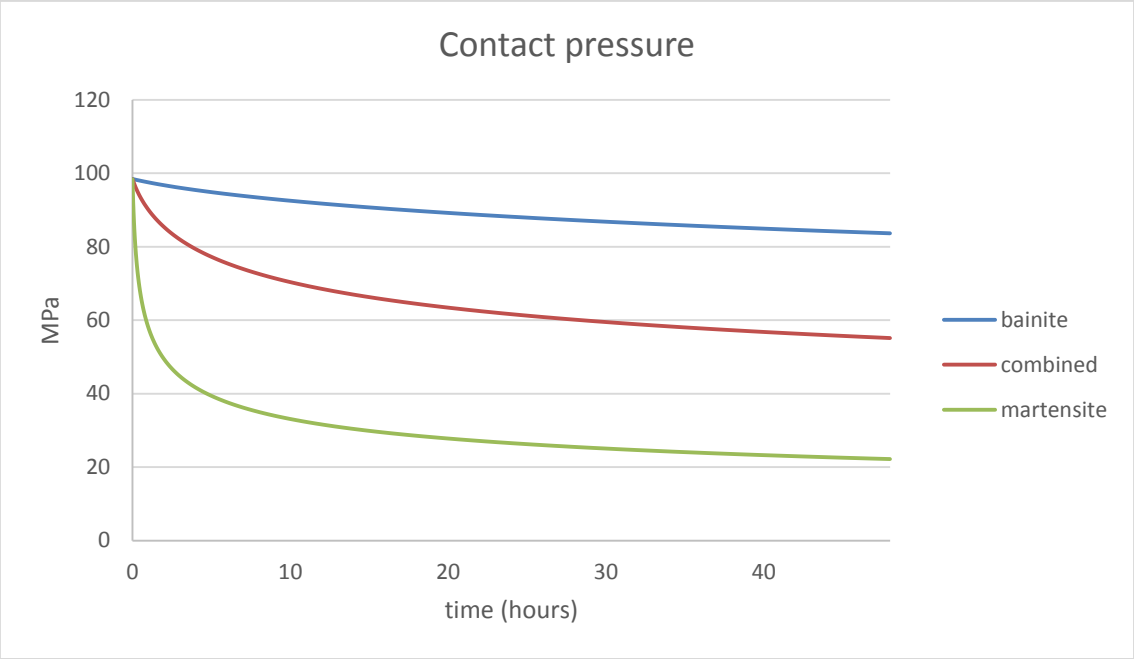

Figure 40 Contact pressure evolution with time

Figure 41 Energy dissipated in the creep process with time

4.2.2 Creep sensitivity analysis

According to some research performed by Dr. Ali Mehmanparast, the power index in the creep law is not affected by changes in temperature, therefore it can be assumed constant when the material remains unchanged. On the other hand, it has been proved that the power law multiplier, *A*, can be described as a function of temperature in most steels [25].

This research was considering 316H steel at a range of temperatures, 550 to 750 in 50 degree Celsius intervals. Table 17 shows creep constants offering the best fit to the simplified creep power law (Equation 7) for his research.

Table 17 316H steel creep constants

Celsius	*A*	*n*
550	1.69E-23	7.51
600	1.03E-21	7.48
650	9.10E-21	7.65
700	6.75E-19	7.44
750	1.35E-17	7.39

Further evaluating the constants, it is confirmed how *n* value stays almost unchanged with temperature. On the other hand, there is a continuous change in *A* value with temperature. The average reduction factor, for this particular steel, every 50 degree interval, is of 28.

The present study will accept this idea, and, keeping *n* unchanged, a sensitivity analysis over the creep multiplier constant, *A*, will be performed. The three materials will take part on this study, comparing the original material properties to materials with power law multipliers reduced by factors of 2, 5, 10 and 28. This final value has been set as an idealized assumption, considering that the rate of change every 50 degrees for a softer steel at higher temperatures is respected for the present conditions. Although this value is not reliable enough, it could serve as an idea of how creep constants would look like at 20 degree Celsius, temperature closer to room temperature than the 70 degree Celsius at which creep properties where obtained. Once again, the purpose of this study is not to precisely quantify creep at room temperature conditions, but to see the possible magnitude, and influence of power law reigning parameters.

In figure 42, bolt preload during a 48-hour period can be seen for the three materials, considering different factors of reduction for the creep multiplier: the original *A*, halved and divided by 5. As it could be expected, the lower the value of the power law multiplier, the lower the creep strain rate, and consequently, the smaller the bolt relaxation. However, once again, the relationship is not straight forward, due to the nature of the relaxation process itself. A halved value of power law multiplier will not result in the same proportion of reduction for the total preload relaxation.

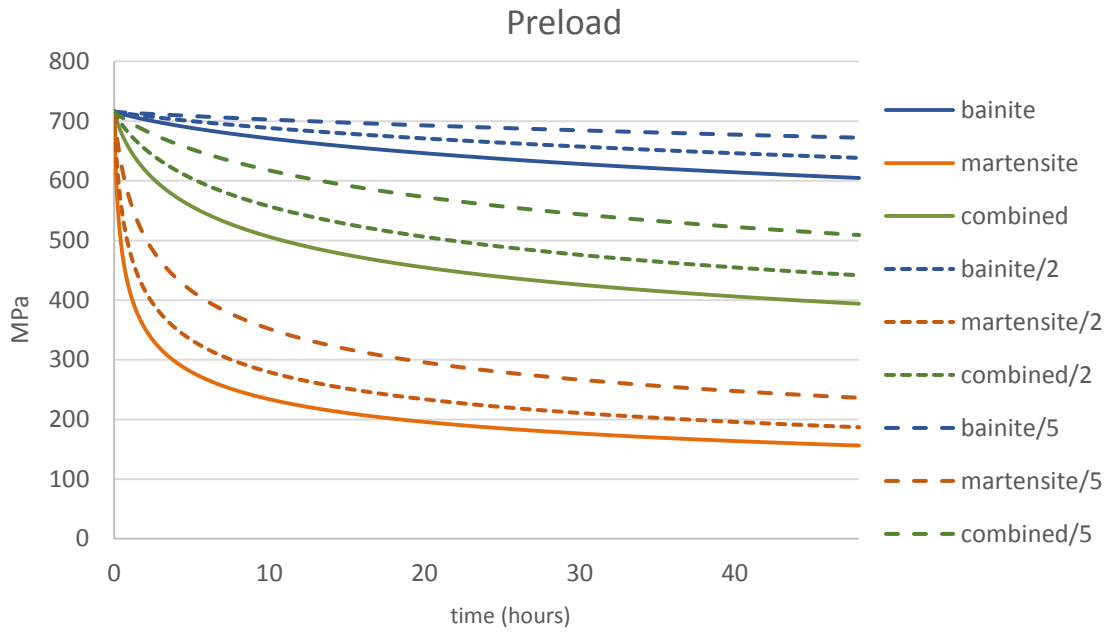

Figure 42 Creep power-law multiplier sensitivity analysis

In the following tables, the variation of preload loss after the 48-hour period can be seen. It is significant how, even for the hardest material with the highest reduction of creep factor, there is still some significant relaxation, close to 2%.

Table 18 Bainite *A* sensitivity analysis

Factor	Preload (0h)	Preload (48 h)	Loss (%)	Ratio
1	717.12	604.74	15.7%	8.83
2	717.12	638.44	11.0%	6.18
5	717.12	672.21	6.3%	3.53
10	717.12	689.32	3.9%	2.19
28	717.12	704.40	1.8%	1.00

Table 19 Combined *A* sensitivity analysis

Factor	Preload (0h)	Preload (48 h)	Loss	Ratio
1	717.12	416.30	41.9%	3.32
2	717.12	441.63	38.4%	3.04
5	717.12	509.08	29.0%	2.30
10	717.12	559.98	21.9%	1.73
28	717.12	626.49	12.6%	1.00

Table 20 Martensite *A* sensitivity analysis

Factor	Preload (0h)	Preload (48 h)	Loss	Ratio
1	717.12	156.14	78.2%	1.60
2	717.12	186.86	73.9%	1.51
5	717.12	236.23	67.1%	1.37
10	717.12	282.21	60.6%	1.24
28	717.12	365.76	49.0%	1.00

All cases show a certain amount of relaxation. Obviously, the martensite model is more sensible to a change in *A* in absolute means, as the percentages of relaxation are remarkably bigger. However, in relative measurements, is the hardest material the one more affected by changes in creep properties.

Hence, it has to be considered that selecting a harder material would positively reduce creep, but there is not enough conclusive information to determine a correlation between preload loss variation and change in *A*.

4.2.3 Load influence on low temperature creep

So far, for all creep simulations, the same conditions have been applied. That is, assuming all surfaces with low friction coefficients (μ=0.14) and a preload equivalent to 90 % of the materials σ_Y. This value of preload, as it was mentioned in section 3.4, is higher than the usual value, recommended to be around 70%. Considering that creep is a tension-dependent phenomenon, the amount of preload applied to the bolt is quite relevant.

Figure 43 shows an analysis of creep conditions for both martensite and the combined material, at loads of 90% and 70% of σ_Y. The amount of relaxation expected is smaller, as $\dot{\varepsilon}_{cr}$ will by the power of *n*. Both scenarios of preloading tend towards the same final load state, both for martensite and combined simulations.

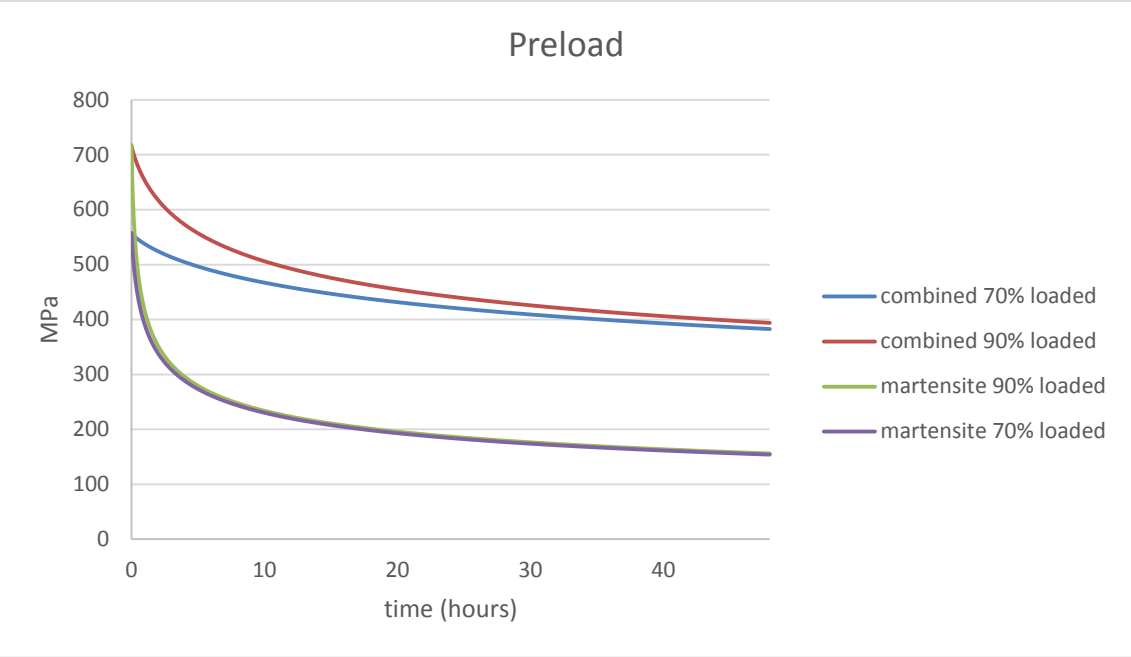

Figure 43 Load level influence on creep

These convergence in results could mean that creep relaxation will be negligible below a minimum load value. They also imply that increasing the load to counter the effects of short-term relaxation might me worthless, at least, regarding the relaxation derived from room temperature creep. It would just slow down the process, but without altering the final state.

Table 21 Relaxation for different loads

	Preload (0h)	Preload (48 h)	Loss (%)	Ratio
combined 70%	555.66	382.65	31%	1.00
combined 90%	717.12	416.30	42%	1.35
martensite 70%	542.81	154.05	72%	1.00
martensite 90%	717.12	156.14	78%	1.09

4.2.4 Friction effects on low temperature creep

Finally, a simple analysis on how friction might affect the amount of relaxation has been performed. As it was explained in section 4.1, friction has a significant influence on the final value of preload that is truly transferred to the bolt. However, this information was obtained by means of a simplified set of tests, which did not consider the instants after the application of the load. Hence, a simple simulation

has been performed, to evaluate if there exists any interaction or correlation between the two effects.

In figure 44, the evolution of total preload of the bolt is shown. As it was previously mentioned, the lower the friction coefficient, the higher the average preload transmitted to the bolt from the tightening process. This is still the case. As time goes on, it can be seen how creep does not really interact with friction, keeping the difference between the two scenarios constant. Therefore, it can be stated that the selection of one condition of friction or another will affect the instant of the application of the preload, but will not influence the effects of RT temperature creep.

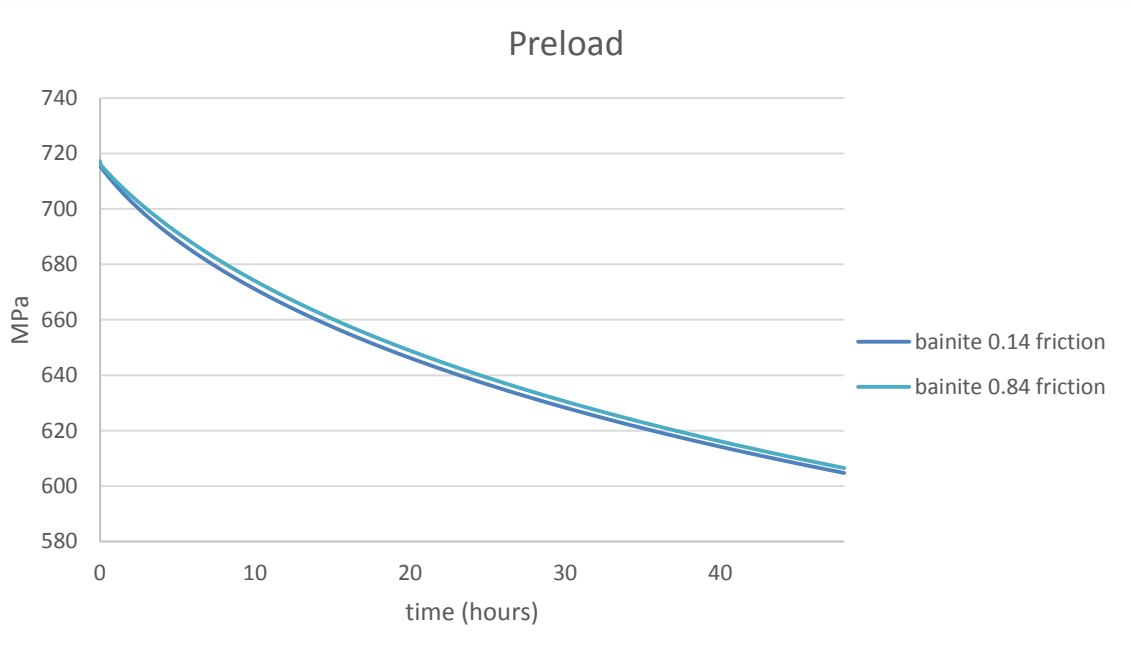

Figure 44 Friction effect on creep

4.2.5 Room temperature creep: Discussion

In the previous sections, some results derived from the creep simulations performed on the model have been presented. These were based on approximated material properties from three different high strength steels, neither of them identical to the steel used for M72 bolts. However, they should give the reader an idea of the phenomenon being analysed. These results are worst-case scenarios, based on maximum creep strain rates, which happen only in the first

instants of creep. Real life experiments should show some creep strain rate reduction with time, due to the hardening of the material.

Therefore, these results should not be considered from a quantitative point of view, as real creep on bolts could differ from these results obtained from the model. However, it could serve as a reference regarding trends and orders of magnitude for RT creep in high strength steel bolts.

The first significant conclusion reached in the present study is that RT creep in bolted connections exists. Even if its creep properties lead to lower $\dot{\varepsilon}_{cr}$ than at high temperatures, the dependency of these strain rates with tensions make that these type of connections, where tensions close to σ_Y are applied, quite critical. Bolted connections are designed to reach tensions of around 70% of σ_Y in the shaft, but tensions will be even higher in some regions that are geometrically more sensitive. That is the case of the thread of both the bolt and the nut.

Consequently, pushing the applied tension in the bolt closer to its σ_Y value (in the present study at around 90 %), would highly increase the tensions, in the main part of the bolt, but also in the thread. Given the power law nature accepted for the creep phenomenon, this increased tension is translated into higher relaxation due to creep.

Following this same line, it is crucial to understand how creep properties of the material affect the creep process itself. From the analysis performed over three different materials, it is visible that stronger materials, those with higher yield stresses, behave better in creep simulations, showing lower relaxation. It has to be noted that plastic properties of the bolt were not changed to match those of the materials from which creep properties were obtained. Hence, plastic deformation after the tightening of the bolt is the same for all the simulations before the apparition of creep.

This means that it might be interesting to select a bolt's material based on not only elastic-plastic behaviour, but also based on short-term criteria given the creep properties of the material. Hence, substituting 10.9 grade steel, whose structure is 90 % martensite with another material more similar to bainite could

be a good choice. Obviously many other factors should be considered, not only creep. So using harder materials working below 70% of yield could help to reduce relaxation effects produced by creep, but without compromising the required clamping for the bolted connection. As shown in figure 43, the final load state after creep relaxation of the bolt depends highly on the material properties, and not on the initial load, converging the different initial preloads towards the same final preload value.

Instead of changing material or altering the load applied on the tightening process, creep properties could be affected in some other ways such as surface hardening, using pinning or some other techniques. A more radical option could as well be using temperature controlled areas around the flanges. Reducing temperature in the joint would reduce the value of the creep power law multiplier, and consequently, total creep. These effect will be proportionally more significant the harder the material. However, reducing temperature, even if it is only a few degrees, would highly increase the risk of brittle fracture.

An analysis of how change of this power law multiplier affects total creep has been performed. Results show that higher strength materials show a higher proportional change in bolt relaxation. However, total change is higher in softer materials, as the order of magnitude of the total relaxation is completely different. Assuming that, once the time component is considered creep rates would be significantly smaller, the main concern will not be the total relaxation, as it will be unavoidable, but the stability of this relaxation. Therefore, materials should be selected so that creep properties are as uniform as possible, in order to minimize preload scatter.

5 CONCLUSIONS

Preload scatter is a major concern in offshore wind industry. From the moment the bolt is released from the tightening tool, some preload is lost. There are several parameters causing this, some known and some unknown, but all them difficult to quantify. The present research has focused on two of them, proving numerically the influence of both friction and low temperature creep. Friction has a direct relation with the total preload transmitted, being desirable to have lower frictions to improve the transformation of preload into actual tension. Lower tensions also contribute to a better distribution of efforts along the threads, showing less risk of plasticity in those threads being more active, whereas having higher stress values in those threads usually inactive with non-lubricated contacts. On the other hand, room temperature creep is not usually considered in a process such as this one. However, the big loads applied for these connections make it necessary. Further experiments are required to define the creep behaviour of these materials under stresses close to yield and at room temperature. From the analysis performed in this document, having materials with higher yield stress working bellow theoretical preload conditions would reduce creep significantly, as staying far from yield in the material would significantly reduce creep.

6 FURTHER WORK

In the following months, several full-scale experiments will be performed at the Structural Integrity Lab in Cranfield University. These experiments will take place in a real flange segment with M72 studs, preloaded with a tensioning tool. The experiments will focus on the effect of different lubricants and coatings in the initial and final values of preload on the studs. Different measurements using ultrasonic tools and strain gages in the middle section of the studs will be taken.

A comparison of the FEA model results and the experimental results would be interesting, in order to confirm the quality of the results of the present study. If this comparison was positive, further simulations could be made, trying to stablish and advanced model correlating friction and preload in bolted connections.These results could as well be helpful to identify the best way to assemble flanged connections of this size in practice. A finding of this type would highly contribute to a reduction of O&M costs in offshore wind turbines.

On the other hand, further tests on room temperature creep should be performed. As there are several factors affecting short-term relaxation in bolted flange connections, the experiments would be highly demanding and of high complexity. Therefore, estimating how much of it is caused by creep would not be easy.

First, creep tests on simple geometry specimens of the material have to be done. These would help to obtain realistic information regarding the creep properties of the material, instead of basing all the results in approximated values. These new models should consider creep as a function of time, reducing $\dot{\varepsilon}_{cr}$ with time, as most experiments show. As an estimation, a time-dependent creep law was created for martensite, based on the same graphs from which maximum values were extracted. The values of the power law constants are shown in table 22.

Table 22 Time dependent creep constants for martensite

A	1.41E-14
n	2.987
m	-0.712

This time dependent model was not considered for the main body of the thesis due to the less accurate fit of the values to the experimental data. Using these new values, results considering and not considering time effects are shown in figure 45. The reduction of the relaxation is quite noticeable, being eight times smaller than that without considering time hardening properties. Even if this same amount of reduction is considered for bainite, creep should still be considered, causing around a 2% of preload loss.

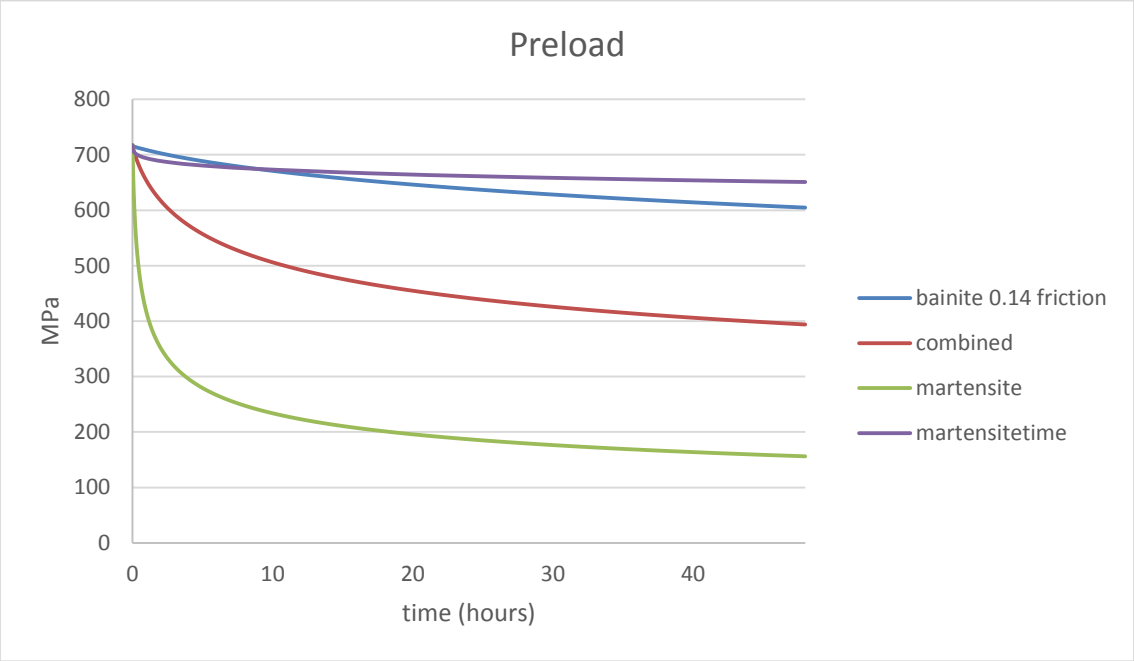

Figure 45 Time dependent creep

Once accurate creep laws were defined for the material, it would be time to perform FEM simulations to determine the real amount of preload loss caused by creep. After this, experiments should take place, using specially machined bolts, with lower-than-average values of roughness, in order to minimize the possible effects of embedment as a source of short-term relaxation.

If these experiments and the simulations were similar, creep caused relaxation could be quantified and confirmed. These could help to determine the major sources of relaxation, which is the first step to properly quantify it and compensate it in real operation.

REFERENCES

1. GWEC. Offshore wind: Global Wind 2016 report. 2016. Available at: http://gwec.net/publications/global-wind-report-2/global-wind-report-2016/ (Accessed: 18 August 2018)

2. Wind Europe., Associates B. Unleashing Europe's offshore wind potential. 2017; (June): 64. Available at: https://windeurope.org/wp-content/uploads/files/about-wind/reports/Unleashing-Europes-offshore-wind-potential.pdf

3. ORE Catapult. Cost Reduction Monitoring Framework 2016 - Summary Report to the Offshore Wind Programme Board. 2017; (January 2016): 20.

4. Stepp M. What Interior's Lease Auction Says about Offshore Wind Innovation. Energy trends insider. 2013. Available at: http://www.energytrendsinsider.com/2013/06/07/what-interiors-lease-auction-says-about-offshore-wind-innovation/ (Accessed: 18 August 2018)

5. Pineda I., Tardieu P. The European offshore wind industry. Wind Europe. 2017; (January): 33. Available at: https://windeurope.org/wp-content/uploads/files/about-wind/statistics/WindEurope-Annual-Offshore-Statistics-2016.pdf

6. Iliopoulos AN., Van Hemelrijck D., Vlassenbroeck J., Aggelis DG. Assessment of grouted samples from monopile wind turbine foundations using combined non-destructive techniques. Construction and Building Materials. Elsevier Ltd; 2016; 122: 855–862. Available at: DOI:10.1016/j.conbuildmat.2015.11.047

7. Industriales I. Retos en la fabricación y cadena de suministro de aerogeneradores offshore. 2016;

8. Rising offshore plant capacities lead to greater data-based O&M gains. New energy update. 2015. Available at: http://newenergyupdate.com/wind-energy-update/rising-offshore-plant-capacities-lead-greater-data-based-om-gains (Accessed: 18 August 2018)

9. Bickford JH. Introduction to the design and behaviour of bolted joints. 4th edn. CRC Press; 2007. 564 p.

10. Kulak GL., Fisher JW., Struik JHA. Guide to design criteria for bolted and riveted joints. American Institute of Steel Construction, Inc. 1988. 1-331 p. Available at: DOI:10.1139/l88-018

11. Shoberg RS. Engineering Fundamentals of Threaded Fastener Design and Analysis. RS Technologies. 2000; : 1–39.

12. FPT. International Technology Roadmap for Test and Test Equipment Summary. 2013;

13. Schwedler M., Dörfeldt S., Lüddecke F., Seidel M., Thiele M. Einflussfaktoren auf die Vorspannkraft von Schrauben mit Durchmessern bis M72 in Ringflanschverbindungen. Stahlbau. 2018; 87(2): 149–161. Available at: DOI:10.1002/stab.201810571

14. K.-H. K. Influence of the Surface State and the Sample Size regarding the Fatigue Strength, VDI-Berichte. 1976. 63-76 p.

15. Screws & bolts.

16. Ranjbar-Far M., Absi J., Mariaux G., Dubois F. Simulation of the effect of material properties and interface roughness on the stress distribution in thermal barrier coatings using finite element method. Materials and Design. Elsevier Ltd; 2010; 31(2): 772–781. Available at: DOI:10.1016/j.matdes.2009.08.005

17. Kassner ME., Perez-Prado M-T. Introduction. Fundementals of Creep in Metals and Alloys. 2004; : 3–9. Available at: DOI:10.1016/B978-008043637-1/50002-8

18. Liu C., Liu P., Zhao Z., Northwood DO. Room temperature creep of a high strength steel. Materials & Design. 2001; 22(4): 325–328. Available at: DOI:10.1016/S0261-3069(00)00074-1

19. 20.2.4 Rate-dependent plasticity: creep and swelling Products:

Abaqus/Standard Abaqus/CAE. 2018; : 1–10.

20. Söderlund A. Influence of Surface Flatness on Bolted Flanges. 2017;

21. Alfredsson B., Arregui IL., Lai J. Low temperature creep in a high strength roller bearing steel. Mechanics of Materials. Elsevier Ltd; 2016; 100: 109–125. Available at: DOI:10.1016/j.mechmat.2016.06.010

22. Information G. Steel grade Transformation temperatures. 2017; : 0–3.

23. Ffs-- LDN. Foundation Flange Study Research Options for WP2. 2018; : 1–23.

24. Concept ITHB., Connection M. CO Cra ID nfie E Cra ID nfie E ld U. (0).

25. Mehmanparast A., Davies CM., Webster GA., Nikbin KM. Creep crack growth rate predictions in 316H steel using stress dependent creep ductility. Materials at High Temperatures. 2014; 31(1): 84–94. Available at: DOI:10.1179/0960340913Z.00000000011

APPENDICES

Appendix A Geometry

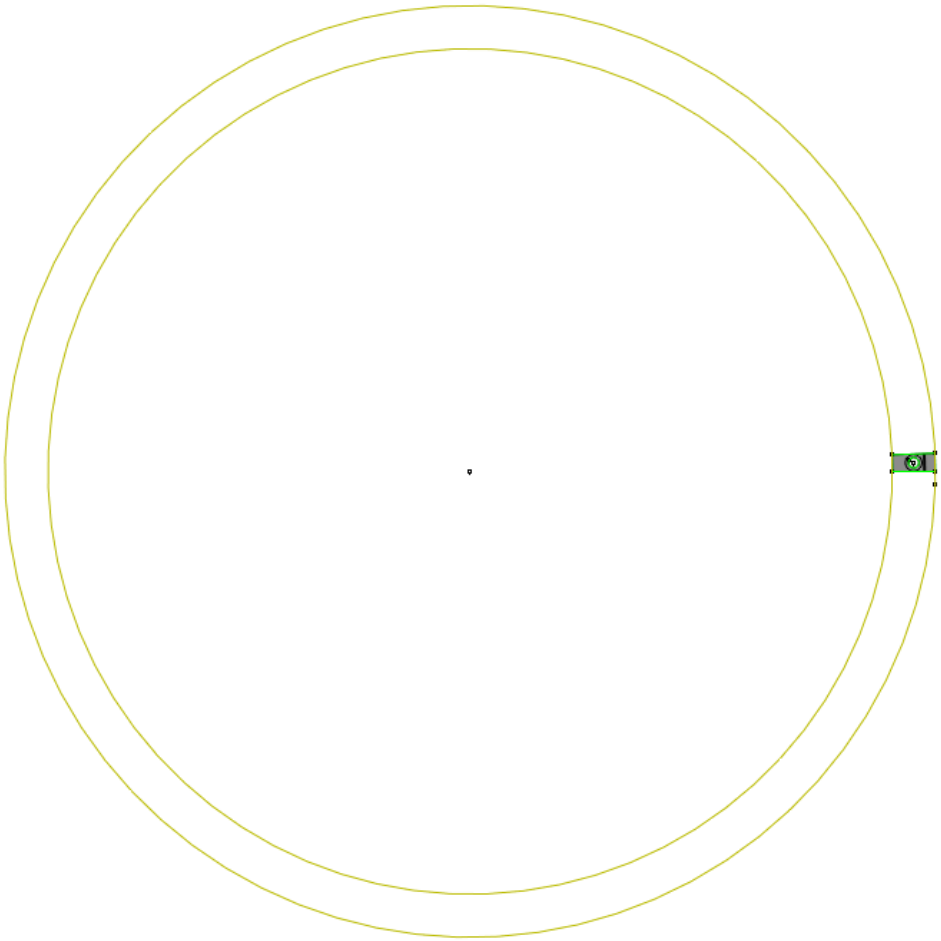

Figure A. 1 Flange CAD drawing

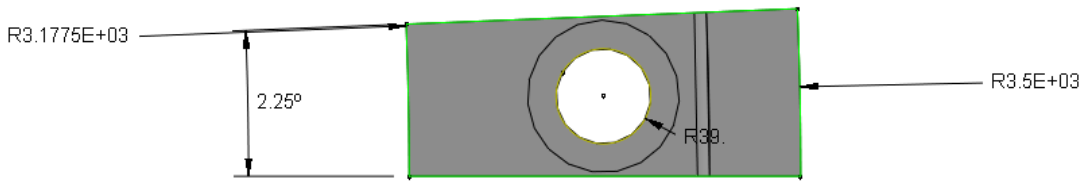

Figure A. 2 Flange segment CAD drawing

Appendix B Mesh

Table B. 1 Total elements in the mesh

Total number of nodes: 851627
Total number of elements: 528930
527350 quadratic tetrahedral elements of type C3D10
1580 linear hexahedral elements of type C3D8R

Table B. 2 Total bolt elements

Total number of nodes: 412894
Total number of elements: 253775
253775 quadratic tetrahedral elements of type C3D10

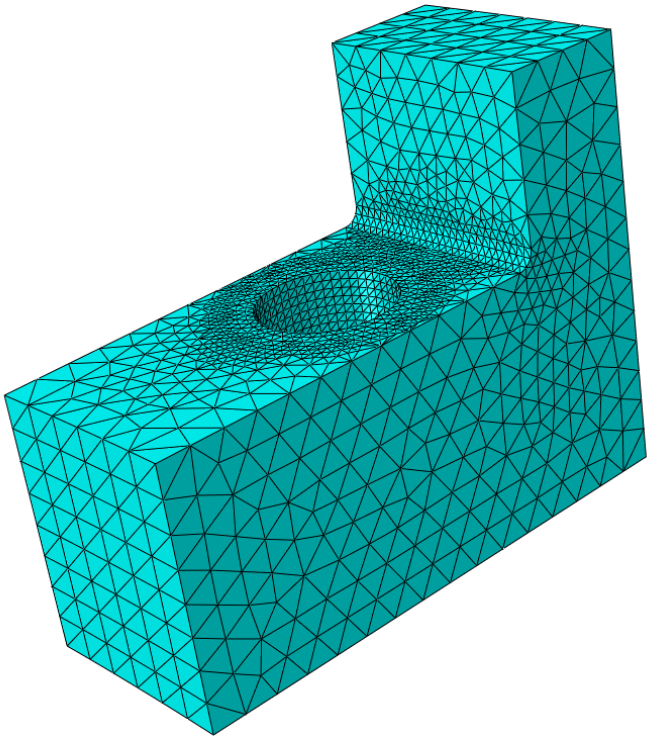

Figure B. 1 Flange mesh detail

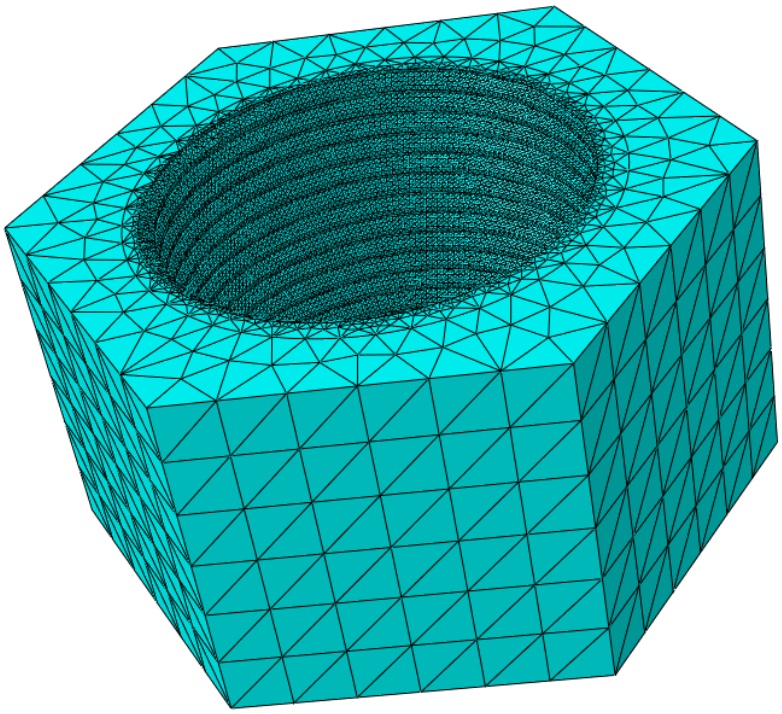

Figure B. 2 Nut mesh detail

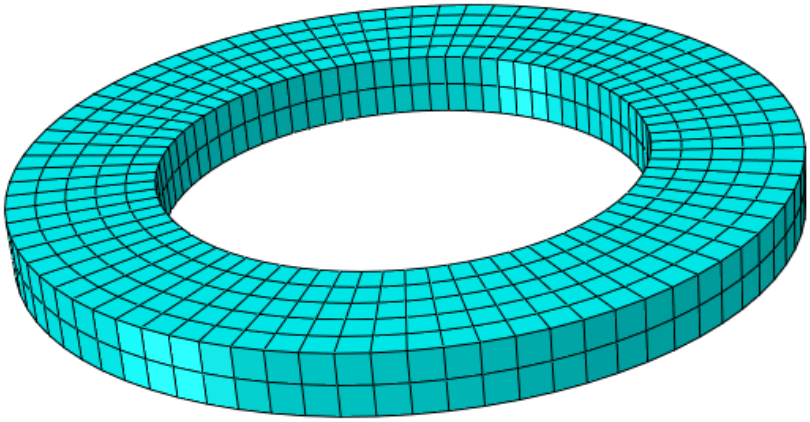

Figure B. 3 Washer mesh detail

Appendix C EXT friction sensitivity analysis

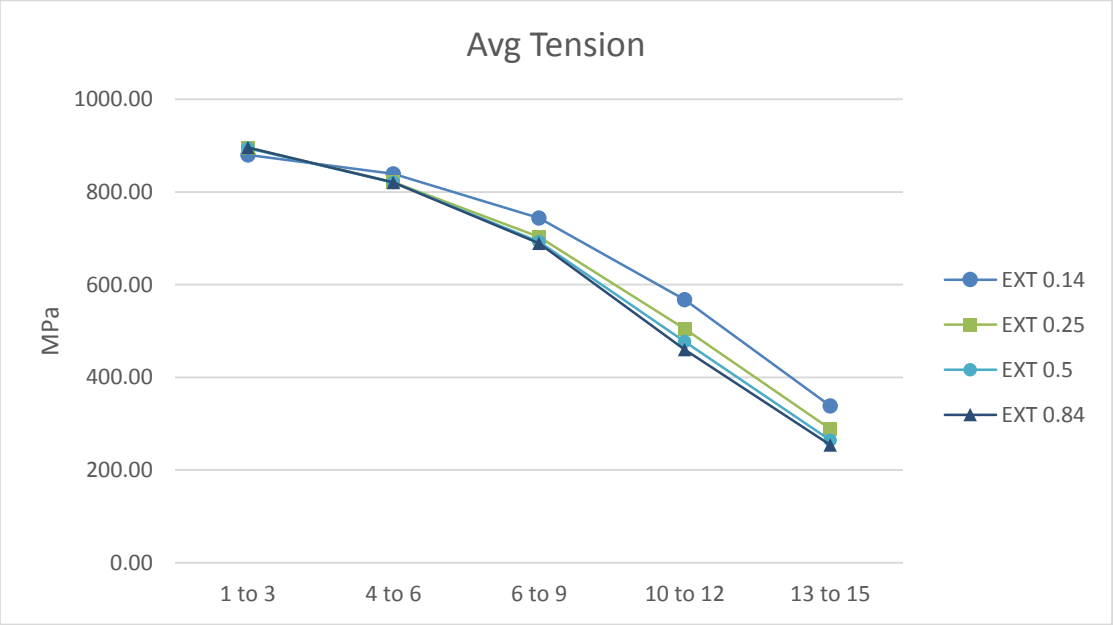

Figure C. 1 Average tensions every three threads TT 0.84

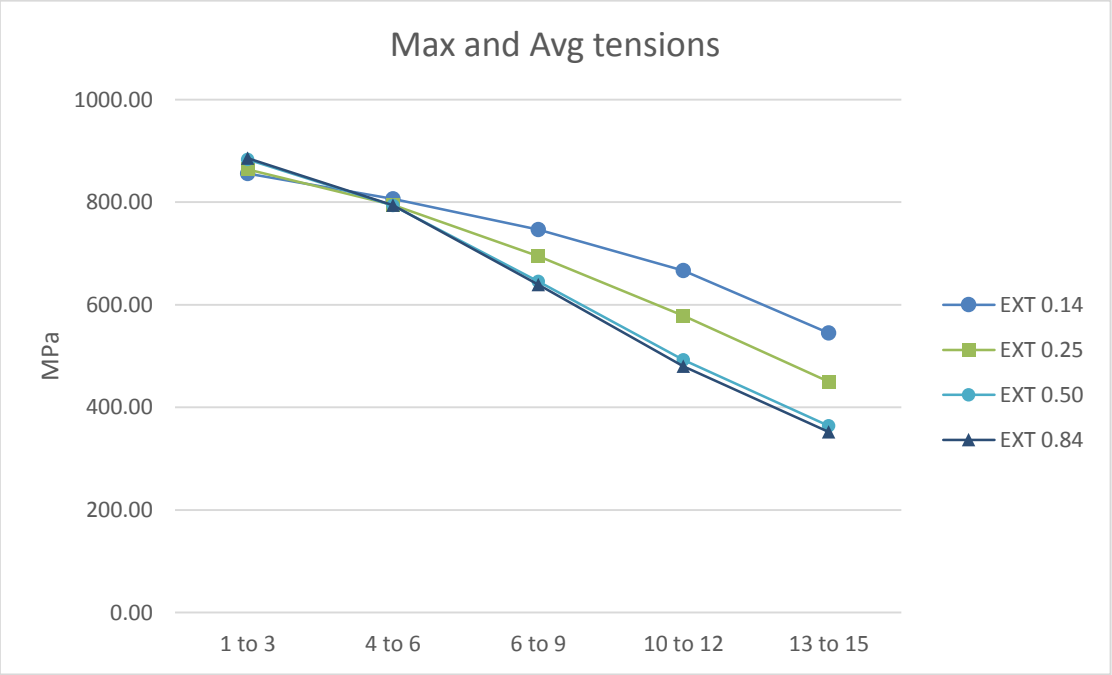

Figure C. 2 Average tensions every three threads TT 0.14

Table C. 1 Maximum tension every three threads TT 0.84 and TT 0.14

	EXT 0.14	EXT 0.25	EXT 0.50	EXT 0.84
1 to 3	1112.43	2.2%	2.1%	2.1%
4 to 6	1092.49	-1.4%	-1.7%	-1.8%
6 to 9	999.42	-2.1%	-2.4%	-2.4%
10 to 12	852.21	-7.7%	-11.5%	-14.3%
13 to 15	512.19	-14.9%	-24.6%	-25.7%
	EXT 0.14	EXT 0.25	EXT 0.50	EXT 0.84
1 to 3	1058.85	0.8%	3.3%	3.7%
4 to 6	1027.01	-1.2%	-1.8%	-1.9%
6 to 9	958.55	-3.0%	-7.0%	-7.6%
10 to 12	916.57	-8.2%	-20.2%	-22.2%
13 to 15	833.86	-15.1%	-30.8%	-33.2%